Cosmological parameter constraints for Horndeski scalar-tensor gravity

Johannes Noller[1,2,*] and Andrina Nicola[2,3,†]

[1]*Institute for Theoretical Studies, ETH Zürich, Clausiusstrasse 47, 8092 Zürich, Switzerland*
[2]*Institute for Particle Physics and Astrophysics, ETH Zürich, 8093 Zürich, Switzerland*
[3]*Department of Astrophysical Sciences, Princeton University, Princeton, New Jersey 08544, USA*

(Received 14 December 2018; published 6 May 2019)

We present new cosmological parameter constraints for general Horndeski scalar-tensor theories, using CMB, redshift space distortion, matter power spectrum and BAO measurements from the Planck, SDSS/BOSS and 6dF surveys. We focus on theories with cosmological gravitational waves propagating at the speed of light, $c_{\rm GW} = c$, implementing and discussing several previously unaccounted for aspects in the constraint derivation for such theories, that qualitatively alter the resulting constraints. In order to ensure our conclusions are robust, we compare results for three different parametrizations of the free functions in Horndeski scalar-tensor theories, identifying several parametrization-independent features of the constraints. We also consider models, where $c_{\rm GW} \neq c$ in cosmological settings (still allowed after GW170817 for frequency-dependent $c_{\rm GW}$) and show how this affects cosmological parameter constraints.

DOI: 10.1103/PhysRevD.99.103502

I. INTRODUCTION

General relativity (GR) at present remains firmly entrenched as a cornerstone of the cosmological standard model. Nevertheless we do know that GR is not the final answer. It is an effective theory that breaks down at Planck energies, is not geodesically complete and is plagued by fundamental problems, most notably the (old) cosmological constant problem. Since GR is the unique consistent theory of a massless spin-2 field (assuming Lorentz invariance), any attempt to modify or extend it in order to address one of these shortcomings will generically introduce new gravitational (light) degrees of freedom (dof). As such, one ought to be on the lookout for any signs of such new *dof*, not just because their detection would revolutionize our understanding of gravity, but also since (in the absence of a detection) this is the most stringent way to test and put constraints on GR itself. With the increasing precision of current and upcoming data, cosmology provides an ideal test bed for the presence of such new gravitational *dof*.

Before contrasting theory with data, one ought to make a choice on how to parametrize potential deviations from GR. Horndeski scalar-tensor theories [1,2] have been the primary workhorse of modified gravity in recent times. They encompass and provide a minimal extension of GR in the sense that only one new single *dof* is introduced, yet this is done with a set of theoretical constraints (notably Lorentz invariance and the absence of higher-derivative ghosts) that ensure one is working with a fundamentally sound theory space. As Horndeski scalar-tensor theories include the vast majority of scalar-tensor theories considered in the literature, but their theory space is nevertheless described by only a few interaction terms in the Lagrangian, these theories provide a simultaneously rich and well-constrained setup in which to place constraints on deviations from GR and the emergence of new gravitational *dof*.

In this paper, we therefore take Horndeski scalar-tensor theories and constrain them using data from several cosmological probes, specifically the cosmic microwave background (CMB) [3,4], baryon acoustic oscillations (BAOs) [5,6], redshift space distortions (RSDs) [7,8] and the matter power spectrum [9]. In the process, we especially focus on the following four questions: (I) What are the cosmological parameter constraints for theories, where gravitational waves propagate at the speed of light, $c_{\rm GW} = c$? (II) What are the corresponding constraints for theories, where the speed of gravitational waves is allowed to differ from that of light? What are the cosmological constraints on $c_{\rm GW}$ then and how does this additional freedom impact constraints on other parameters? (III) Horndeski theories are spanned by four free functions, each in principle requiring an infinite number of parameters to be fully specified.[1] One therefore needs to choose a more restrictive and specific ansatz for these functions in order to

*johannes.noller@eth-its.ethz.ch
†anicola@astro.princeton.edu

[1]Note that a number of known extensions to Horndeski scalar-tensor theories exist, which introduce higher-order derivatives in the equations of motion, yet do not propagate additional ghostly degrees of freedom due to degeneracies/hidden constraints in those specific theories. Examples include so-called "beyond Horndeski" [10] and DHOST [11,12] theories, which introduce a small number of additional free functions (especially at the level of linear perturbations, which we will discuss in detail here).

efficiently extract cosmological constraints. What parametrization(s) should one choose and what cosmological constraints are robust under a change of parametrization? (IV) What datasets provide the most stringent constraints? Do they preferentially point towards specific modified gravity theories and are there (hints of) deviations from GR? What additional theoretical priors should one impose?

Outline: This paper is organized as follows. In Sec. II, we recap Horndeski scalar-tensor theories, their linearly perturbed action and how these can be significantly simplified by requiring gravitational waves to propagate at the speed of light, $c_{\rm GW} = c$ (as extensively discussed in the wake of GW170817 and GRB 170817A). In Sec. III, we then consider different parametrizations for the remaining functional freedom and discuss them alongside additional theoretical (stability) constraints. This is followed by an overview of the different datasets used to extract cosmological parameter constraints in Sec. IV. In Sec. V we then present the constraints for theories with $c_{\rm GW} = c$, discuss what essential aspects drive the constraints and how to best interpret the results, what constraints are robust under changes of parametrizations and what they mean for dark energy/modified gravity theories. In Sec. VI, we recap cosmologically relevant caveats in the argument that infers $c_{\rm GW} = c$ from GW170817 and GRB 170817A, which imply that $c_{\rm GW} \neq c$ is still a valid setup on cosmological scales. We discuss how constraints change, if the speed of gravitational waves is allowed to vary, and present the corresponding Monte Carlo Markov Chain (MCMC) analysis. Finally, we conclude in Sec. VII and provide further details in the Appendices.

Notation and conventions: Since we will be considering scalar-tensor theories, the principal ingredients will be a tensor $g_{\mu\nu}$ and a scalar ϕ. The covariant derivative associated with $g_{\mu\nu}$ is ∇_μ and we will introduce the shorthand $\Phi_{\mu\nu} \equiv \nabla_\mu \nabla_\nu \phi$. Finally, angular brackets denote taking the trace, so, e.g., $[\Phi] = \Phi_\mu{}^\mu$ and $[\Phi^2] = \Phi_{\mu\nu}\Phi^{\mu\nu}$.

II. HORNDESKI GRAVITY

Here we briefly summarize the essential features of Horndeski scalar-tensor theories in a gravitational context, how they are defined, what free functions span the associated theory space and how these can be efficiently captured at the level of the linearized action.

A. Horndeski scalar tensor-theories

The most general Lorentz-invariant scalar-tensor action that gives rise to second-order equations of motion (and is consequently free of an Ostrogradski-ghost instability by default), is Horndeski gravity [1,2][2]:

$$S = \int d^4x\sqrt{-g}\left\{\sum_{i=2}^{5}\mathcal{L}_i[\phi, g_{\mu\nu}]\right\}, \tag{1}$$

where the $\mathcal{L}_i$ are scalar-tensor Lagrangians given by:

$$\begin{aligned}
\mathcal{L}_2 &= G_2(\phi, X),\\
\mathcal{L}_3 &= -G_3(\phi, X)[\Phi],\\
\mathcal{L}_4 &= G_4(\phi, X)R + G_{4,X}(\phi, X)([\Phi]^2 - [\Phi^2]),\\
\mathcal{L}_5 &= G_5(\phi, X)G_{\mu\nu}\Phi^{\mu\nu} - \frac{1}{6}G_{5,X}(\phi, X)([\Phi]^3\\
&\quad - 3[\Phi^2][\Phi] + 2[\Phi^3]).
\end{aligned} \tag{2}$$

Four free functions (G_2, G_3, G_4, G_5) therefore completely characterize this theory. The G_i are functions of a scalar field ϕ and its derivative via $X \equiv -\frac{1}{2}\nabla_\mu\phi\nabla^\mu\phi$.[3] Finally, $G_{i,\phi}$ and $G_{i,X}$ denote the partial derivatives of the G_i with respect to ϕ and X, respectively.

In the aftermath of the near simultaneous detections of GW170817 and GRB 170817A [14–18] it was shown in [19–22] that imposing $c_{\rm GW} = c$ in a cosmological context significantly reduces the full Horndeski theory space (2), namely by eliminating G_5 and $G_{4,X}$, as we will discuss in the next subsection. Note that we will revisit this argument in Sec. VI, where we recap why extrapolating the measurement of $c_{\rm GW} = c$ from GW170817 and GRB 170817A to a cosmological context requires additional nontrivial assumptions and we discuss varying $c_{\rm GW}$ models in setups where these assumptions do not hold. Putting this issue aside for the time being, imposing $c_{\rm GW} = c$ in a cosmological context reduces Horndeski theory to

$$S = \int d^4x\sqrt{-g}\{G_2(\phi, X) - G_3(\phi, X)[\Phi] + G_4(\phi)R\}, \tag{3}$$

where there are now only three free functions left (G_2, G_3, G_4) and G_4 is a function of ϕ only.[4] For previous related work on $c_{\rm GW} = c$ constraints see [24–33].

B. Linearized perturbations

With a cosmological setting in mind, the general Horndeski action (1) can be expanded around a spatially

[2]See [13] for the equivalence between different formulations.

[3]The fact that the Lagrangian only depends on the first derivative via X is a consequence of Lorentz invariance.

[4](3) is essentially of the kinetic gravity braiding form [23]. Note that imposing $c_{\rm GW} = c$ for cosmology only enforces $G_{5,X} = 0$, if the scalar *dof* affects the cosmological background evolution, as it certainly should if it is at all related to dark energy/modified gravity. However, this does mean, that for theories where the scalar is sufficiently suppressed and does not affect cosmological evolution, $G_{5,X} = 0$ may be consistently violated [21], as is the case for Einstein-dilaton-Gauss-Bonnet theories (EdGB), that are of interest e.g., in strong gravity phenomenology.

flat homogeneous and isotropic background. Doing so to quadratic order in the (linear) perturbations yields the linearized dynamics of [34–37]—also see [13,38,39]. Here we will not repeat the derivation of the associated action, but instead note that the dynamics of linearized perturbations is completely controlled by four functions [34]: They are the effective Planck mass M_S and its running α_M, the kineticity α_K that contributes to the kinetic energy of scalar perturbations, the braiding α_B that quantifies the strength of kinetic mixing between scalar and tensor perturbations, and the tensor speed excess α_T, which is related to the speed of sound of tensor perturbations c_T via $c_{\rm GW}^2 = 1 + \alpha_T$. In terms of the model functions G_i these are given by [34]

$$\begin{aligned} M_S^2 &\equiv 2(G_4 - 2XG_{4,X} + XG_{5,\phi} - \dot{\phi}HXG_{5,X}), \\ HM_S^2\alpha_M &\equiv \frac{d}{dt}M_S^2, \\ HM_S^2\alpha_B &\equiv 2\dot{\phi}(XG_{3,X} - G_{4,\phi} - 2XG_{4,\phi X}) \\ &\quad + 8XH(G_{4,X} + 2XG_{4,XX} - G_{5,\phi} - XG_{5,\phi X}) \\ &\quad + 2\dot{\phi}XH^2(3G_{5,X} + 2XG_{5,XX}), \\ M_S^2\alpha_T &\equiv 2X[2G_{4,X} - 2G_{5,\phi} - (\ddot{\phi} - \dot{\phi}H)G_{5,X}], \end{aligned} \tag{4}$$

where all the G_i as well as ϕ and X are evaluated for the background configuration. We further use the shorthand $G_i \equiv G_i(\phi, X)$ and refer to [34] for the (lengthy) expression for α_K.

These expressions greatly simplify when we specialize to the restricted Horndeski theories (3) with luminally propagating gravitational waves. In that case, one trivially obtains $\alpha_T = 0$ and, collecting results for the α_i, we obtain

$$\begin{aligned} M_S^2 &= 2G_4, \\ HM_S^2\alpha_M &= \frac{d}{dt}M_S^2, \\ H^2M_S^2\alpha_K &= 2X(G_{2,X} + 2XG_{2,XX} - 2G_{3,\phi} - 2XG_{3,\phi X}) \\ &\quad + 12\dot{\phi}XH(G_{3,X} + XG_{3,XX}), \\ HM_S^2\alpha_B &= 2\dot{\phi}(XG_{3,X} - G_{4,\phi}), \\ \alpha_T &= 0. \end{aligned} \tag{5}$$

Note that, as before, all parameters are determined in terms of the three free functions (G_2, G_3, G_4), where G_4 is a function of ϕ only and (G_2, G_3) can be functions of both ϕ and X.

III. PARAMETRIZATIONS AND STABILITY CONDITIONS

The α_i functions discussed above map the functional freedom from the full Horndeski action (captured by G_2, G_3, G_4, G_5) into their physically relevant combinations at the level of the linearized action. In order to extract meaningful constraints for these functions, it is necessary to reduce their inherent functional freedom by using some parametrized form for these functions. Indeed this is also the approach implemented in state-of-the-art Einstein-Boltzmann solvers for Horndeski theories, such as hi_class [40] and EFTCAMB [41]. The purpose of such parametrizations is to capture the dark energy evolution to reasonable accuracy in the late-universe. While naturally most simple parametrizations will not be able to capture the complex behavior of fully-fledged dark energy theories at all times, they should nevertheless recover leading-order effects affecting late universe physics. We emphasize that such parametrized and model-independent searches should be seen as an initial coarse tool to identify promising regions of theory space. Specific fundamental theories in these regions can subsequently be further analyzed in more targeted searches.

A. Parametrizing the background

In general Horndeski theories, there is sufficient functional freedom such that the Hubble rate H can be set independently of the α_i [34].[5] Motivated by the observed proximity of the background expansion to ΛCDM, in what follows we will therefore follow the minimal approach of [42,43] and fix the background to be that of ΛCDM, considering and constraining perturbations around this background.[6]

The background equations read

$$H^2 = \rho_{\rm tot}, \qquad \dot{H} = -\frac{3}{2}(\rho_{\rm tot} + p_{\rm tot}), \tag{6}$$

where "tot" denotes a sum over all components contributing to the background dynamics (explicitly including the dark energy component) and we note the specific choice of units employed by CLASS and hi_class, especially $8\pi G = 1$ and a rescaling of all densities and pressures by a factor of 3.

B. Parametrizing linear perturbations: The α_i

Different parametrizations for the α_i are discussed in [34,42–48]. These parametrizations have been used in

[5]Note that this does not mean that this can be done for any subclass of Horndeski. In quintessence theories, for example, any nontrivial dynamics is associated with a (small) departure from ΛCDM at the background level already. This is somewhat analogous to how slow-roll solutions in inflationary theories are never exactly de Sitter.

[6]We leave an extended analysis simultaneously constraining deviations from ΛCDM at background and perturbation levels (and using the observational datasets considered here) to future work. Since (as we will see below) current constraints on the α_i are $\mathcal{O}(1)$, whereas the background is known to more closely resemble ΛCDM, it is in any case a reasonable first step to compute constraints on the α_i without also varying the background.

Refs. [42,43,49–53] to both compute and forecast parameter constraints. However, conclusions about observational constraints on dark energy obtained assuming a specific parametrization will always be open to the question to what extent that conclusion depends on the specific parametrization chosen. In order to disentangle physical effects and artefacts of choosing specific parametrizations, we will therefore compute constraints for three different parametrizations (already implemented in HI_CLASS), which we now summarize:

Parametrization I: A one-parameter ansatz, where the α_i scale with $\Omega_{\rm DE}$

$$\alpha_i = c_i \Omega_{\rm DE}, \tag{7}$$

where we emphasize that $\Omega_{\rm DE}$ here refers to the time-dependent fractional energy density of dark energy, not its value at one specific given time. Linking the parametrization to $\Omega_{\rm DE}$ ensures that the modification to GR only becomes relevant once dark energy provides a sizeable fraction of the background energy density. This parametrization is known to accurately capture the evolution of a wide sub-class of Horndeski theories [54,55], but not all [45]. The effective Planck mass M_S^2 is inferred from the parametrized α_M via integrating $HM_S^2\alpha_M \equiv \frac{d}{dt}M_S^2$.

Parametrization II: An alternative one-parameter ansatz, with all α_i proportional to the scale factor

$$\alpha_i = c_i a. \tag{8}$$

The dependence on the scale factor ensures that the modification switches off smoothly at early times (recall that $\alpha_i = 0$ is the GR limit) and is a feature shared by the third parametrization below as well. We note that a initially grows more quickly than $\Omega_{\rm DE}$, which only begins to increase at a faster rate than the scale factor around $z = 1$, before flattening out eventually. Therefore, dark energy perturbations become relevant slightly earlier in parametrization II than in parametrization I. As before, the effective Planck mass M_S^2 is inferred from the parametrized α_M via integrating $HM_S^2\alpha_M \equiv \frac{d}{dt}M_S^2$.

Parametrization III: A two-parameter ansatz, where all α_i scale with powers of a, except for α_M, which is implicitly parametrized via the deviation of the effective Planck mass from (the constant) $M_{\rm Pl}$. Explicitly, we have

$$\alpha_j = c_j a^{n_j}, \quad \frac{M_S^2}{M_{\rm Pl}^2} = 1 + c_{\delta M} a^{n_{\delta M}}, \quad \alpha_M = \frac{c_{\delta M} n_{\delta M} a^{n_{\delta M}}}{M_S^2}, \tag{9}$$

where the index j runs over $\{B, K, T\}$, i.e. braiding, kineticity and gravitational wave speed contributions and the expression for α_M follows from that for M_S^2. Since the time-dependence of each α_i is freed up individually, different α_i need no longer be proportional to one another here. A two-parameter ansatz (for each α_i) such as (9) has been argued to be well-suited for extracting the maximal information from present data [46]. Here we in effect choose the asymptotic late-time value as well as the rate at which the modification switches on, independently for each α_i.

These three parametrizations are suitably rich and different, that any conclusion invariant under a switch between them should be relatively robust and therefore parametrization-independent. At the same time, considering different parametrizations will also allow us to get an understanding of which features are a consequence of choosing a specific parametrization, rather than a conclusion enforced by the data themselves.

C. Stability conditions

Imposing stability conditions on the parameters of the theory serves two purposes. First, observationally relevant instabilities would exclude the associated parameter values in any case, so checking for their potential presence before computing the full cosmology in an MCMC run increases computational efficiency, but does not alter the result. Gradient instabilities are frequently of this type. Second, some instabilities may not show up in the classical analysis one performs in an MCMC run, but nevertheless undermine the validity of the theory (e.g., once quantum effects are taken into account). Ghost instabilities can be of this type, leading to an exponential decay of the vacuum that any purely classical analysis would be blind to. Checking whether ghost instabilities are present therefore safeguards against accidentally including theories that are ill-defined at a fundamental level.

We will impose the standard stability conditions implemented by hi_class. These are first ghost-freedom conditions for the scalar and tensor mode, respectively given by

$$\alpha_K + \frac{3}{2}\alpha_B^2 > 0, \qquad M_S^2 > 0. \tag{10}$$

If these were broken in the linear theory already, this is the sign of a fatal instability for the theory. Note that for Horndeski theories the no-ghost condition is explicitly k-independent, so a would-be ghost is present at all scales/energies here. In more general modified gravity theories k-dependence can enter into a no-ghost condition [37], in which case a more careful analysis of the precise nature of the ghost is required (e.g., small k ghosts have been argued to be harmless in [56]).

Second, we impose the absence of gradient instabilities, i.e. a positive speed of sound (effectively this amounts to considering the large-k limit of the "mass" term in Fourier space and requiring this term to be positive). In Horndeski theories with $\alpha_T = 0$, i.e. for (3), the condition for the absence of a tensor mode gradient instability is trivially satisfied, while the scalar mode condition is given by

$$c_s^2 = \frac{1}{\alpha_K + \frac{3}{2}\alpha_B^2} \cdot \left[(2-\alpha_B)\left(\frac{1}{2}\alpha_B + \alpha_M - \frac{\dot{H}}{H^2}\right) - \frac{3(\rho_{\rm tot} + p_{\rm tot})}{H^2 M_S^2} + \frac{\dot{\alpha}_B}{H} \right] > 0. \quad (11)$$

Using the background equations (6), we will find it useful to recast this condition in the equivalent form

$$c_s^2 = \frac{1}{\alpha_K + \frac{3}{2}\alpha_B^2} \cdot \left[(2-\alpha_B)\left(\frac{1}{2}\alpha_B + \alpha_M\right) + \frac{2\dot{H}}{H^2}\left(\frac{1-M_S^2}{M_S^2}\right) + \frac{\frac{d}{dt}(\alpha_B H)}{H^2} \right] > 0. \quad (12)$$

These conditions need to be modified, if the speed of gravitational waves is left undetermined. In this case, the absence of gradient instabilities for the tensor mode requires

$$\alpha_T \geq -1, \quad (13)$$

while for the scalar mode the gradient stability condition becomes

$$c_s^2 = \frac{1}{\alpha_K + \frac{3}{2}\alpha_B^2} \cdot \left[(2-\alpha_B)\left(\frac{1}{2}\alpha_B(1+\alpha_T) + \alpha_M - \alpha_T - \frac{\dot{H}}{H^2}\right) - \frac{3(\rho_{\rm tot} + p_{\rm tot})}{H^2 M_S^2} + \frac{\dot{\alpha}_B}{H} \right] > 0. \quad (14)$$

We emphasize that using the above gradient stability conditions to exclude parameter space in exploring theories ought to be used with caution. Cosmologies with significant such classical instabilities will automatically be excluded by the data, when exploring the full parameter space with an MCMC run. While it is computationally more efficient to only explore a reduced parameter space based on the above stability cuts, one ought to be careful not to place overzealous cuts and exclude physically viable parameter space (thus biasing the results). We have therefore checked for a number of cases that constraints with and without gradient stability priors indeed only show very mild differences, so using the above cuts is well-justified. Tachyon instabilities and the associated stability conditions, on the other hand, are far more involved (for a discussion see [37,57,58]), especially since the presence of such instabilities can in fact be required to ensure the physical validity of a model (the Jeans instability is the prime example here). We therefore choose a maximally safe approach and do not exclude any parts of parameter space based on tachyonic stability cuts *a priori*, but instead let the data exclude any cosmologies with significant such instabilities. While this approach is less computationally efficient, it guards against biasing our results by only sampling part of the physically viable parameter space.

TABLE I. Overview of the datasets considered in this work.

Acronym	Description	Reference
P15	Constraints from Planck Collaboration 2015, TT + lowP	[3]
P15 + lensing	Constraints from Planck Collaboration 2015, TT + lowP and CMB lensing convergence.	[3,4]
BAO	BAO measurements from BOSS and SDSS. SDSS DR7: $z_{\rm eff} = 0.15$, $D_V(z_{\rm eff}) = (664 \pm 25) r_d / r_{d,\rm fid}$ Mpc BOSS DR11: $z_{\rm eff} = 0.32$, $D_V(z_{\rm eff}) = (1264 \pm 25) r_d / r_{d,\rm fid}$ Mpc	[5,6]
RSD	RSD constraints from BOSS and 6dF. BOSS DR11: $z_{\rm eff} = 0.57$, $D_V(z_{\rm eff})/r_d = 13.85 \pm 0.17$, $F(z_{\rm eff}) = 0.6725 \pm 0.0283$, $f(z_{\rm eff})\sigma_8(z_{\rm eff}) = 0.4412 \pm 0.0435$ 6dF: $z_{\rm eff} = 0.067$, $f(z_{\rm eff})\sigma_8(z_{\rm eff}) = 0.423 \pm 0.055$	[7,8]
mPk	Constraints from SDSS DR4 LRG power spectrum shape	[9]

IV. DATA AND THEORETICAL MODELLING

In order to constrain general Horndeski scalar-tensor theories, we combine several different datasets, which are illustrated in Table I and detailed below.[7]

A. Data

CMB: We use CMB temperature and polarization data from Planck's second data release [3,59,60].[8] Specifically, we include low-ℓ ($2 \leq \ell \leq 29$) temperature and polarization data as well as high-ℓ ($30 \leq \ell \leq 2508$) temperature data in form of the published Planck likelihood. In our fiducial setup, we analyze high-ℓ temperature data using the PLIK LITE likelihood, which has been marginalized over all nuisance parameters except for the Planck absolute

[7]We note that there exist many datasets additional to the ones discussed below. In this work, we choose a conservative approach and exclude any datasets that could be correlated to each other, as they probe the same underlying structures.

[8]We note that, while this work was being finalized, the Planck Collaboration published its final results. The most significant difference between these and the earlier results from 2015 is the shift to a lower value of the optical depth to reionization, $\tau_{\rm reion}$, by approximately 1.5σ. As there are no strong correlations between the value of $\tau_{\rm reion}$ and the α_i parameters, we believe that these new constraints will not significantly affect our conclusions.

calibration parameter.[9] We further complement these measurements with the Planck CMB lensing likelihood [4] in the angular multipole range $40 \leq \ell \leq 400$.

RSD: We include two complementary RSD measurements in our analysis. As a first dataset, we use the RSD measurement derived from BOSS DR11 CMASS anisotropic clustering at an effective redshift $z_{\rm eff} = 0.57$ [8]. Further, we also include the RSD measurement at $z_{\rm eff} = 0.067$ obtained from 6dF galaxy clustering data in Ref. [7].

BAO: We complement the above datasets with isotropic BAO measurements from BOSS and SDSS. Specifically we include constraints on the volume averaged distance D_V at $z_{\rm eff} = 0.32$ from BOSS DR11 LOWZ data [5] and BAO measurements at $z_{\rm eff} = 0.15$ from the SDSS DR7 main sample [6]. Note that we exclude the anisotropic BAO measurement from CMASS, which is also given in Ref. [5], as it is highly correlated with the RSD measurement of Ref. [8]. Reference [6] showed that the cross-correlations between the RSD and BAO datasets included in this work are negligible and we thus assume all these datasets to be independent.

mPk: Finally we include constraints on the shape of the matter power spectrum (mPk) at $z_{\rm eff} = 0.35$ from SDSS DR4 luminous red galaxies (LRG) [9]. Ref. [9] measured the galaxy clustering power spectrum $P_{gg}(k)$ in three-dimensional Fourier space for 20 k-bands in the range $0.01h$ Mpc$^{-1} < k < 0.2h$ Mpc^{-1}. In our analysis, we only consider k-bands with $k < 0.1h$ Mpc^{-1} in order to minimize sensitivity to nonlinear clustering and scale-dependent bias.

B. Theoretical modeling

We compute theoretical predictions for all observables considered using the publicly-available code HI_CLASS[10] [40], which extends the Boltzmann code CLASS[11] [61] to subsets of Horndeski scalar-tensor theory [1]. For CMB and BAO data we follow the implementations described in Refs. [4,5,8,60]. Detailed explanations of theoretical modeling choices employed for RSD and matter power spectrum data are given in Appendix A.

V. COSMOLOGICAL PARAMETER CONSTRAINTS

We derive constraints on cosmological parameters in a joint fit to the data discussed in Sec. IV. We make the simplifying assumption that the cross-correlations between all datasets are negligible,[12] and we therefore assume a joint Gaussian likelihood as

$$\mathcal{L}(D|\boldsymbol{\theta}) = \mathcal{L}_{\rm CMB}(D_{\rm CMB}|\boldsymbol{\theta})\mathcal{L}_{\rm RSD}(D_{\rm RSD}|\boldsymbol{\theta}) \cdot \mathcal{L}_{\rm BAO}(D_{\rm BAO}|\boldsymbol{\theta})\mathcal{L}_{\rm mPk}(D_{\rm mPk}|\boldsymbol{\theta}), \quad (15)$$

where $\boldsymbol{\theta}$ denotes the vector of model parameters and D_i a given data vector. We sample $\mathcal{L}(D|\boldsymbol{\theta})$ in a Monte Carlo Markov Chain (MCMC) with the publicly-available code MONTEPYTHON[13] [62,63], using the Metropolis-Hastings algorithm [64,65]. We set the background cosmological model to ΛCDM and, in addition to the parameterization-dependent modified gravity parameters detailed in Sec. III, vary the six cosmological parameters $\{w_{\rm cdm}, w_{\rm b}, \theta_{\rm s}, n_{\rm s}, \log 10^{10} A_s, \tau_{\rm reion}\}$, where $w_{\rm cdm} = \Omega_{\rm cdm} h^2$ is the fractional cold dark matter density today, h is the Hubble parameter, $w_{\rm b} = \Omega_{\rm b} h^2$ is the fractional baryon density today, $\theta_{\rm s}$ is the position of the first peak in the CMB temperature anisotropy power spectrum, $n_{\rm s}$ denotes the scalar spectral index of initial perturbations, $A_{\rm s}$ is the primordial power spectrum amplitude at a pivot scale of $k_0 = 0.05$ Mpc^{-1} and $\tau_{\rm reion}$ denotes the optical depth to reionization. We also suppress the tensor-to-scalar ratio, setting $r = 0$, and impose that the asymptotic value of the effective Planck mass M at early times is indeed $M_{\rm Pl}$, since we do not wish to constrain early universe modifications of gravity (for a different approach, see [42]). Following Ref. [3], our fiducial model includes two massless and a massive neutrino eigenstate and we fix the sum of their masses to the minimal mass allowed by oscillation experiments, i.e. $\sum_\nu m_\nu = 0.06$ eV. In addition to the cosmological parameters, we further vary three nuisance parameters $\{A_{\rm Planck}, b, n\}$, where $A_{\rm Planck}$ denotes the Planck absolute calibration parameter, b is a linear, redshift-independent galaxy bias parameter and n parametrizes systematic uncertainties due to shot noise and nonlinear evolution in the matter power spectrum (for more details, see Appendix A). When extracting parameter constraints we check for convergence, in particular ensuring the Gelman-Rubin

[9] We have tested the impact of this choice, by rerunning our analysis for a fiducial ΛCDM background cosmology using the full Planck high-ℓ temperature likelihood (with all of its additional nuisance parameters) instead of the premarginalized PLIK LITE likelihood. Constraints obtained using the full Planck high-ℓ temperature likelihood and ones obtained using the PLIK LITE likelihood agree very well—see Appendix B for details. Note that this was to be expected, due to the explicit choice of a ΛCDM background cosmology in our analysis—see the discussion in Sec. III.

[10] The code can be found at: http://miguelzuma.github.io/hi_class_public/.

[11] The code can be found at: http://class-code.net.

[12] This assumption is justified for the BAO and RSD datasets, as we have not included any potentially correlated BAO or RSD datasets in our analysis. In addition, CMB and LSS probes are weakly correlated due to the ISW effect, which is therefore a potentially constraining probe of general modified gravity theories. We therefore expect that our constraints can only improve upon inclusion of these cross-correlations and leave a detailed investigation thereof to future work.

[13] The code can be found at: http://baudren.github.io/montepython.html.

diagnostic [66] R satisfies $R-1 \lesssim 0.01$ for all (cosmological and nuisance) parameters.

A. Constraining the α_i

In the following, we show parameter constraints for the α_i functions that parametrize departures from GR for various combinations of the datasets listed in Table I and for the different α_i-parametrizations, (7), (8) and (9). In this section we assume luminally propagating gravitational waves, so work with (3) as the underlying action. Theories with $c_{\rm GW} \neq c$ will be discussed in Sec. VI. Constraints shown are marginalized over all standard ΛCDM and nuisance parameters as discussed above. The reader is referred to Appendix B for further details on parameter constraints for these standard parameters and consistency checks.

1. The constrainable α_i parameter space

Out of the four α_i, it is important to note that α_K is in effect the combination of the G_i and their derivatives that is "orthogonal" to the parameter space probed by linear cosmology and therefore hardly constrained by the data used here [42].[14] For the purposes of the analysis here, one can consequently fix α_K to an essentially arbitrary fiducial parameter, and we will do so in what follows.[15] In addition, we highlight that $\alpha_B = 2$ is a singular point in the α_i parameter space[16] in the following sense: When computing the linear theory around a Friedmann-Robertson-Walker (FRW) background in the context of Horndeski models (1), one may focus on the scalar perturbations of the metric and the scalar ϕ, expand the action to quadratic order in these perturbations, gauge fix and integrate out auxiliary variables (for details, see [37]). This procedure results in a kinetic term for the scalar perturbation $\delta\phi$ of the following form

$$\mathcal{L}^{(2)}_{\rm kin} \propto \frac{(3\alpha_{\rm B}^2 + 2\alpha_{\rm K})H^2 M_S^2 \dot{\delta\phi}^2}{(\alpha_{\rm B}-2)^2}. \tag{16}$$

Clearly the kinetic term diverges when $\alpha_B = 2$. This is because setting $\alpha_B = 2$ eliminates mixing between the metric perturbations Φ and B in the action, turning B into a Lagrange multiplier—for details we again refer to [37]. As a result, the $\alpha_B = 2$ theory propagates no gravitational scalar degree of freedom and no physical model should therefore evolve across this boundary, as this would imply a discontinuity in the number of propagating *dof*. In the parameter plots we are about to discuss, we will therefore explicitly mark the $\alpha_B = 2$ line whenever relevant and forbid evolution across this boundary.[17]

2. Parametrization I: $\alpha_i = c_i \Omega_{\rm DE}$

Constraints for this parametrization are shown in Fig. 1. First, we note that the sharp, lower (small c_M) boundary of the contours is due to the onset of gradient instabilities. For the CMB-only constraints, the other boundaries are mostly determined by the late integrated Sachs-Wolfe (ISW) effect. The ISW especially excludes cosmologies with large c_M or c_B, as these lead to the generation of too much power for the low-ℓ C_ℓ^{TT}, which can be seen in Fig. 3. This is in good agreement with the observation of [40] that modifications to the late ISW are indeed the driving factor in CMB constraints on the c_i—also see [49]. Note that from CMB constraints alone there is a "degeneracy direction" roughly satisfying $c_M \sim 2.5 c_B$ for small c_M, where the effect of the c_i conspires to avoid large power for the low-ℓC_ℓ^{TT}. Adding BAO and mPk data only very mildly improves constraints, whereas RSD constraints on $f\sigma_8$ rule out large, positive c_M values. Finally note that the singular $\alpha_B = 2$ case discussed above does not appear here, as in this parametrization and for $\Omega_{\rm DE,0} \sim 0.7$, $\alpha_B = 2$ today corresponds to $c_B \sim 2.86$ (or progressively larger as one goes back in time) and these high-c_B cosmologies are already strongly disfavored by Planck CMB constraints.

3. Parametrization II: $\alpha_i = c_i a$

As can be seen from Fig. 1, analogously to above, the CMB-only constraints lie along a "degeneracy direction," which in this parametrization is given by $c_b \sim 1.8 c_M$. Also as before, BAO and mPk data do not add significant additional constraining power. The contours around the degeneracy direction are tightened in comparison with the $\alpha_i = c_i \Omega_{\rm DE}$ parametrization discussed above, resulting in a correspondingly tighter correlation between c_M and c_B—departures away from this direction lead to large excess power on large scales again. Also in contrast to the first parametrization, all negative c_M values are ruled out by requiring the absence of gradient instabilities in this parametrization. Finally notice that constraints not including RSDs in fact favor large values of c_B and c_M, driving chains in the analysis to preferentially explore regions close to the singular point $\alpha_B = 2$ (which is crossed in the past for $c_B > 2$). Combined with a somewhat bimodal distribution for both c_i when only using these datasets, this leads to

[14] This is related to the findings that (I) at leading order, α_K does not affect the dynamics in the quasistatic approximation and (II) very large scale modes (sensitive to relativistic effects) have a much smaller statistical weight on constraints for the α_i than smaller scale modes (for which quasistatic approximation holds to high accuracy) [43].

[15] We have checked that our results do not change for a wide variety of fiducial choices for α_K. For concreteness we have chosen $c_K = 0.1$ for all the results shown here. n_K, in the context of parametrization III, has been fixed to $n_K = 3$.

[16] We thank Emilio Bellini for several discussions related to this point.

[17] Note that the plots in Figs. 1 and 2 present binned data, so any points seemingly just over the $\alpha_B = 2$ boundary appear as such as an artefact of the binning.

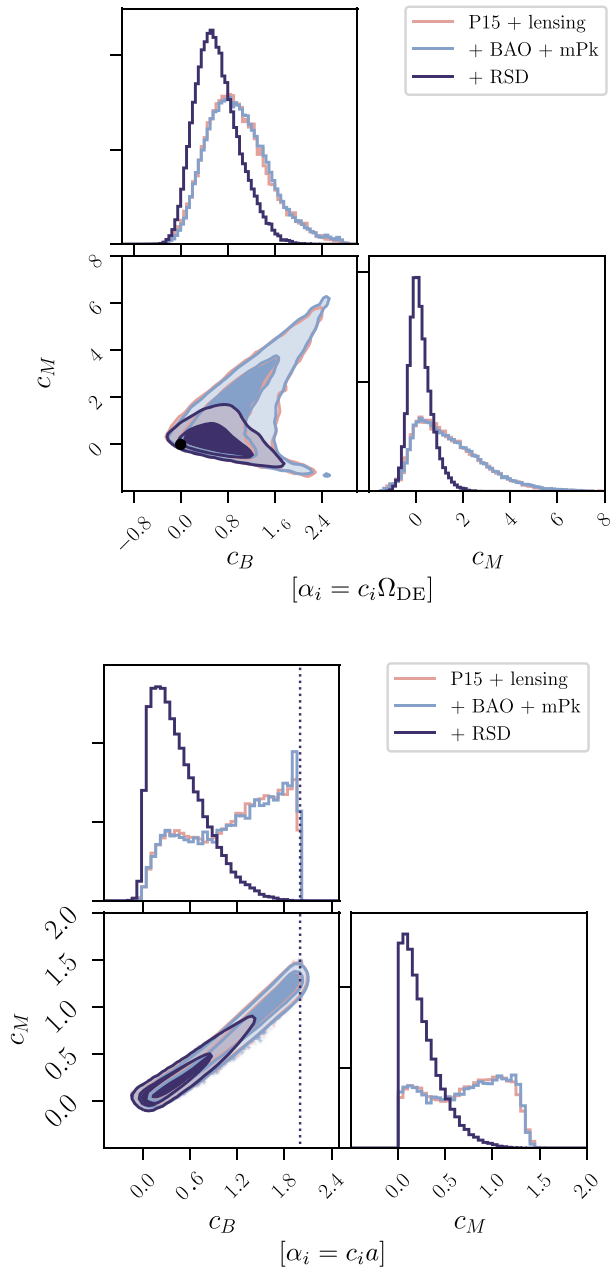

FIG. 1. Cosmological parameter constraints for the modified gravity c_i parameters, using parametrizations I (7) ($\alpha_i = c_i \Omega_{\rm DE}$) and II (8) ($\alpha_i = c_i a$). The inner (outer) contours correspond to 68% (95%) confidence levels, respectively and we plot results for different combinations of the datasets detailed in Sec. IV above. The lower (negative) c_M boundary is due to the onset of gradient instabilities. Otherwise, without RSD data, the shape of the contours is primarily driven by the late ISW effect in the low-ℓ CMB temperature anisotropy power spectrum C_ℓ^{TT} (also see Fig. 3). Once RSDs are taken into account, their measurement of $f\sigma_8$ establishes a strong upper bound for c_M, thus strengthening constraints. Finally note one additional feature for the (8) parametrization (right panel). All models with $c_B > 2$ here will cross the singular $\alpha_B = 2$ point in their past evolution (for the left panel this would correspond to $c_B \sim 2.86$, so does not affect constraints there) and we consequently do not explore such models, as discussed below.

slowly converging chains for these cases. However, RSDs rule out large c_B, c_M values, thus driving the preferred values for the c_i back closer to GR and removing any bimodality.

4. Parametrization III: $\alpha_j = c_j a^{n_j}$

The constraints for parametrization III are shown in Fig. 2. In order to correctly interpret the results, recall that $M_S^2 \alpha_M = c_{\delta M} n_{\delta M} a^{n_{\delta M}}$ here, so the analogue to c_M in the previous parametrizations is $c_{\delta M} n_{\delta M}$, not $c_{\delta M}$. We first note that we impose an upper bound on the n_i, namely $n_i \leq 20$, as large n_i essentially remove any observable cosmological effect of the α_i by suppressing them until very late times.[18] Large n_i cosmologies are therefore indistinguishable from standard ΛCDM in practice, so that MCMCs will not converge unless an upper bound is placed on the n_i. This is particularly manifest in the constraints for n_B. $n_{\delta M}$ is far better constrained, precisely for the above reason that c_M in the above parametrizations is analogous to $c_{\delta M} n_{\delta M}$ here, so $n_{\delta M}$ inherits some of the constraining power acting on c_M. In addition, removing the proportionality between α_M and α_B removes any significant correlation between $c_{\delta M}$ and c_B. This can be seen by noting that $c_{\delta M}$ is still driven to low values by RSD constraints, as before, but this does not lead to a corresponding tightening of constraints on c_B here. c_B is only weakly affected by adding RSD constraints and for all datasets prefers values close to the singular $c_B = 2$ point. Note that parameter constraints using this parametrization have also been derived and discussed in [49]. Our analysis differs from the results presented there in two important aspects. First, we take into account additional modified gravity effects on $f\sigma_8$ in our analysis (see Appendix A), resulting in stronger constraints from RSDs. Second, as discussed in Sec. III, we do not exclude models that display tachyonic instabilities. Since such instabilities can be an essential part of well-motivated physical models, we simply let the data decide which models to accept. In this way one is sure to avoid introducing unphysical biases as artefacts of overzealous stability priors. Overall the differences in the analysis have a strong effect on the parameter constraints obtained: [49] found that the posterior for $c_{\delta M}$ (or $\tilde{M}_0$ in the notation used in [49]) displayed strong bimodality and was predominantly driven away from its GR value zero, as a result of tachyonic instabilities.[19] Our analysis shows no such bimodality for the $c_{\delta M}$ posterior, qualitatively changing constraints on the running of the Planck mass in comparison to [49], with the best-fitting cosmologies clustered

[18]Negative n_i introduce large modifications at early times, so we do not discuss this case, since we are focusing on late-time modifications here. The precise upper bound on n_i is arbitrary, but we have chosen $n_i \leq 20$ to facilitate the comparison with [49].

[19]We thank Christina Kreisch for related discussions.

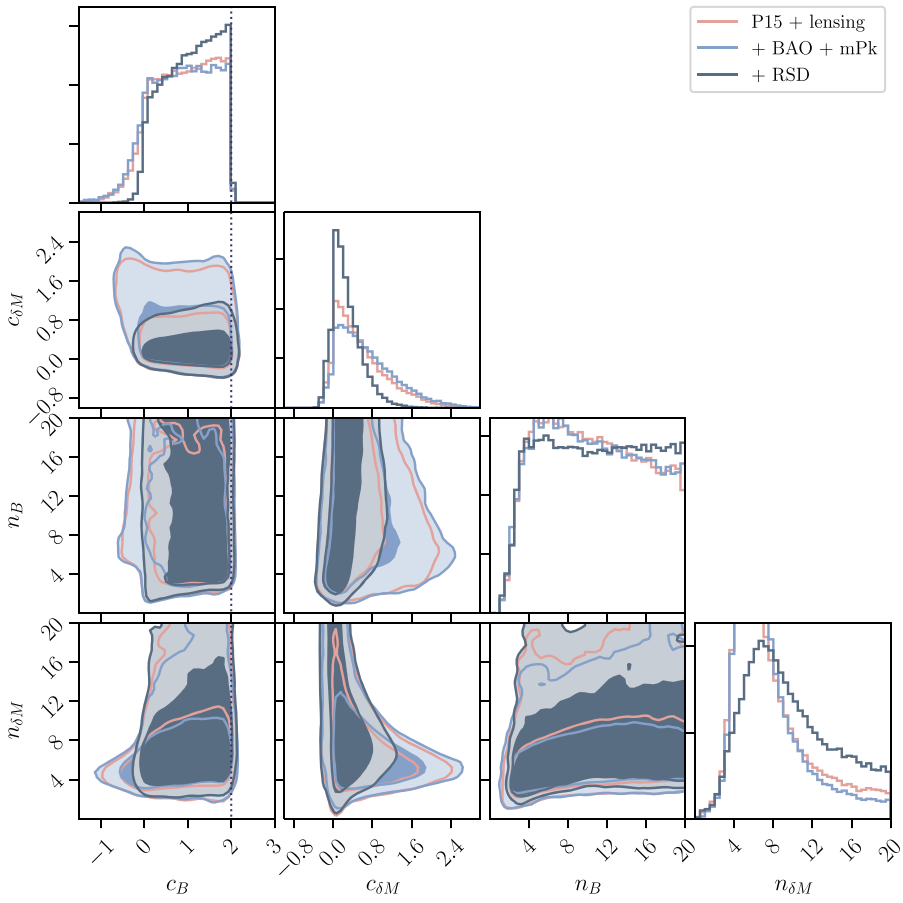

FIG. 2. Cosmological parameter constraints for the modified gravity parameters in parametrization III (9). The inner (outer) contours correspond to 68% (95%) confidence levels, respectively and we plot results for the same datasets as in Fig. 1. In close analogy to that figure, c_M is tightly constrained, whereas freeing up the power-law dependence on c_B weakens the constraints for that parameter, illustrating that the c_B constraints in Fig. 1 where significantly strengthened by choosing a parametrization for which $\alpha_B \propto \alpha_M$. Also again notice the singularity cut for $c_B = 2$. We impose bounds for the poorly constrained power-law parameters $n_i \leq 20$, since the analysis will not converge otherwise: Arbitrarily large n_i correspond to suppressing modified gravity effects until extremely late in the evolution, so very large n_i yield near-identical cosmological phenomenology. The constraint for $n_{\delta M}$ is stronger than that for n_B, since in this parametrization $c_{\delta M} n_{\delta M}$ is analogous to c_M in the above parametrizations—recall that here $\alpha_j = c_j a^{n_j}$ and $M_S^2 = M_{\rm Pl}^2(1 + c_{\delta M} a^{n_{\delta M}})$ so $M_S^2 \alpha_M = c_{\delta M} n_{\delta M} a^{n_{\delta M}}$.

around the GR value for this parameter. As can be seen from Fig. 2, this change in posterior for $c_{\delta M}$ also qualitatively changes the constraints for the other parameters, removing any strong suppression for large values of $n_{\delta M}$ in the associated posterior (and similarly removing any suppression for large values of n_B in its posterior).

B. What drives the constraints?

Constraining power on the α_i primarily comes from three sources:

(i) CMB constraints limit deviations from GR by effectively placing an upper bound on the α_i. Large α_i in all parametrizations are generically associated with too much power for the C_ℓ^{TT} on large scales (small ℓ) due to a modified late ISW effect. In the context of the $\alpha_i = c_i \Omega_{\rm DE}$ parametrization, this was already discussed in [40] and is explicitly shown in Fig. 3 for a number of illustrative choices of the c_i and their corresponding cosmologies.

(ii) The onset of gradient instabilities, associated to the stability condition (11), rule out large negative values for both α_i.

(iii) RSD data further reduce the allowed α_M, as can be seen from Fig. 4. If α_M is closely correlated/proportional to α_B, this results in analogously strong constraints on α_B.

For the CMB constraints, note that we used the high-ℓ, low-ℓ *and* lensing likelihoods for Planck 2015.[20] Constraints in

[20]We note that the addition of the lensing likelihood is crucial to obtain optimal constraints—we have checked for a fiducial cosmology that pure CMB constraints are significantly weakened without the lensing likelihood.

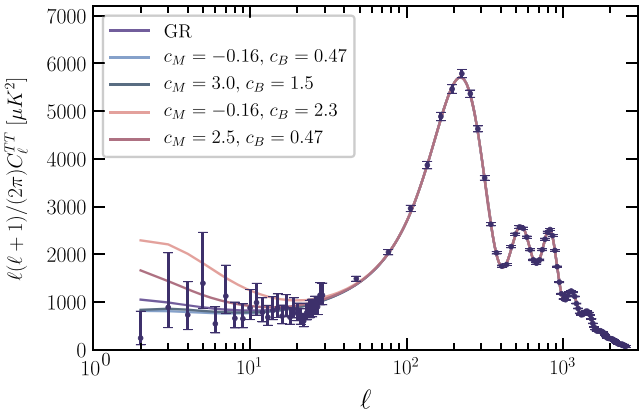

FIG. 3. Illustration of the effect of modified gravity parameters on the CMB TT power spectrum. The data points used in this work are shown with 1σ uncertainties (specifically, the uncertainties shown correspond to the square root of the diagonal elements of the covariance matrix of the data and thus do not include potential correlations between the data points) and we plot a standard ΛCDM/GR cosmology as well as four other cosmologies with nonvanishing c_i. Since we focus on the effects of the c_i, all standard ΛCDM parameters are fixed to their Planck 2015 best-fit values here [3]. Note that the second ($c_M = -0.16$, $c_B = 0.47$) cosmology corresponds to the best-fit values we obtain for these parameters in our MCMC analysis for the $\alpha_i = c_i\Omega_{\rm DE}$ parametrization (although the corresponding cosmology here is close to, but not identical, to that best-fit, since we impose the Planck best-fit choices for all other parameters). The third cosmology shows that there is a "degeneracy" direction associated with simultaneously enlarging c_M and c_B from CMB constraints alone (and only for "small" c_i, see Fig. 1). The final two cosmologies illustrate that individually increasing c_M or c_B eventually leads to too much added power on large scales via the late ISW effect.

general are only mildly improved by further adding BAO and mPk data. For BAOs this is due to the fact that we have fixed the background to be ΛCDM. As the angular diameter distance and the Hubble scale (as constrained by the BAO data used here) are background quantities, adding BAO data does not directly add constraining power for the modified gravity c_i parameters. The constraining power of mPk on the c_i is also rather weak. This is because, for the scales considered in our analysis, the c_i mainly affect the amplitude of the matter power spectrum, as can be seen from Fig. 4, and this effect is degenerate with both galaxy bias and the amplitude of fluctuations. For implementation details see Appendix A.

The addition of RSD constraints primarily affects c_M, ruling out large values for this parameter. This is because $f\sigma_8$, as constrained by RSD measurements, traces the growth of structure on the associated scales, which strongly depends on the effective strength of gravity. This is predominantly determined by the effective Planck mass, which is increased at late times by larger c_M values. So the growth of structure as measured by the growth function f is significantly more limited when including RSD data than with CMB constraints alone. In addition there is also an additional smaller effect on c_B and effects on H_0 and σ_8, which we will discuss in Appendix B. Note that fully propagating modified gravity effects in mapping RSD constraints onto bounds on the c_i (via $f\sigma_8$) is important for extracting the full constraining power of RSDs on the modified gravity parameter space we investigate here (see Appendix A). Finally, recall that we use two sets of RSD data, namely samples from the BOSS and 6dF surveys. Interestingly both surveys individually add similar constraining power in terms of the α_i parametrization

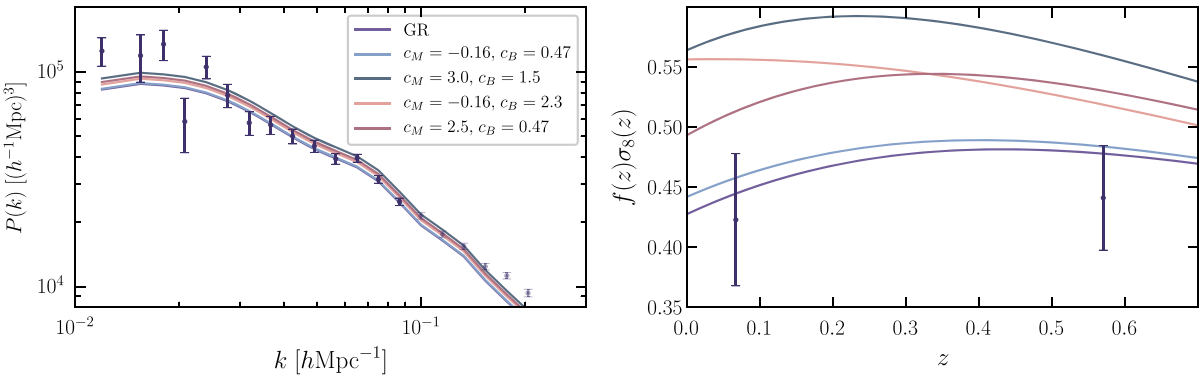

FIG. 4. Illustration of the effect of modified gravity parameters on the matter power spectrum and $f\sigma_8$. The data points used in this work are shown with 1σ uncertainties as before and we plot the same set of cosmologies as in Fig. 3. The matter power spectrum (left plot) only weakly discriminates between the different cosmologies used here, due to a degeneracy between galaxy bias and the c_i in their effects on the amplitude of the power spectrum. We emphasize that shaded data points are excluded from our analysis, since their correct interpretation requires modeling nonlinearities in a way that takes into account nonlinear modified gravity effects (which we do not). $f\sigma_8$ constraints from RSDs (right plot), on the other hand, have strong constraining power. In this context we highlight the second and third cosmology, which yield very similar CMB TT power spectra (see Fig. 3), but very different signatures for $f\sigma_8$. As a result, the third (large c_M) cosmology is strongly disfavored by RSDs.

parameters, with the BOSS RSD data being marginally more constraining.

C. Robust conclusions

Having considered the constraints for individual parametrizations above, we would now like to extract those conclusions that are generic and independent of the choice of parametrization (at least within the representative set of parametrizations we have considered here).

1. Parametrization-independent conclusions

For all parametrizations, α_M can at most be mildly negative due to gradient instability constraints. This places a tight limit on how much smaller than $M_{\rm Pl}$ the effective Planck mass M_S can be. Depending on the functional form of/parametrization chosen for α_M this can be strengthened up to ruling out negative α_M altogether (e.g., in parametrization II). Similarly, while all parametrizations considered above allow mildly negative α_B, positive α_B is always preferred at the 2σ level (see Table II). If $\alpha_M \propto \alpha_B$, then the parametrizations tested suggest that Planck + BAO + mPk constraints generically yield a preferred direction in the associated c_M, c_B plane (see parametrizations I and II in Fig. 1), at least for small α_i/c_i. This is of interest in the context of models, where this proportionality is a genuine feature of the model (e.g., for the Horndeski subclasses discussed in [54,55], whose dynamics are very accurately captured by parametrization I) and not just an artefact of the parametrization. Including RSD data always reduces the allowed parameter range for α_M by ruling out large positive values. This can also further restrict α_B, but only if it is sufficiently closely correlated to α_M, e.g., if they are proportional to one another (whether this is true is model/parametrization-dependent).

2. Deviations from GR?

Since negative values of $\alpha_{M,B}$ are strongly constrained by the onset of gradient instabilities, GR occupies a special place in the $\alpha_{M,B}$ plane. In other words, observationally admissible departures from GR are not symmetric in this plane.[21] In all parametrizations $\alpha_M = 0$ provides a good fit to the data. When considering only its marginalized constraints, α_B mildly prefers departures from GR at roughly 2σ confidence level (see Table II). Note, however, that any statement on model selection needs to take into account both the full parameter space of a given model and its number of degrees of freedom. Since a parametrized analysis as performed here is blind to the true number of underlying fundamental parameters and degrees of freedom, we do not perform any model selection analysis in this work. Finally note that imposing additional theoretical constraints, e.g., as motivated by radiative stability [67], has a tendency to eliminate additional non-GR parameter space and therefore tends to drive parameters closer to their GR values. So any apparent tension with GR, for a given parametrization, may at least partially be due to incomplete information about the underlying models and should therefore be interpreted with caution.

[21]Note that this in fact applies for all theories with $\alpha_M = 0 = \alpha_B$. Also, it is instructive to focus on the c_i in testing "convergence" to GR. In the first two parametrizations considered here this is trivial, but note that for the third parametrization ($\alpha_i = c_i a^{n_i}$), while $n_i \to \infty$ in a sense recovers GR-like phenomenology for arbitrary c_i, it is much cleaner to focus on $c_i \to 0$ as the GR limit of this parametrization as well.

TABLE II. Constraints on the modified gravity parameters for the different parametrizations used in this work. Note that we do not include the n_i parameters of parametrization III (9) here, since these are only very poorly constrained—see Fig. 2. The uncertainties/limits quoted denote the 95% c.l.. In the final parametrization, c_T has a highly skewed, non-Gaussian posterior (see Fig. 5), so we only give an upper limit at the 95% c.l. for this parameter. For a detailed comparison with previous work, taking into account the use of different datasets and theoretical priors, see Secs. V and VI.

Parametrization	Parameter	Posterior
I	c_B	$0.63^{+0.83}_{-0.62}$
	c_M	$0.20^{+1.15}_{-0.82}$
II	c_B	$0.48^{+0.83}_{-0.46}$
	c_M	$0.27^{+0.54}_{-0.26}$
III	c_B	$1.1^{+0.89}_{-1.1}$
	$c_{\delta M}$	$0.30^{+0.77}_{-0.45}$
I (c_T free)	c_B	$0.71^{+0.88}_{-0.71}$
	c_M	$-0.01^{+1.3}_{-0.87}$
	c_T	< 0.26

VI. RESURRECTING $c_{\rm GW} \neq c$ FOR COSMOLOGY

Inferring the equality of the speed of gravitational waves and the speed of light for cosmological energy scales $H_0 \sim 10^{-33} eV$ from the measured equality of those speeds for GW170817 and GRB 170817A (measured at energy scales $\sim 10^{-13} eV$) implicitly assumes a scale/time/energy-independent speed of gravitational waves. As such, this caveat also applies to the derivation of (3). Importantly, and as pointed out by [68], this means the energy scale probed by GW170817 is significantly larger than that of late-universe cosmology and lies very close to the naive cutoff of theories involving a G_3 interaction, usually taken to be $\Lambda_3 = (M_{\rm Pl} H_0^2)^{1/3} \sim 10^{-13} eV$. Making a measurement at those scales therefore in principle tests the (unknown and possibly partial) UV completion of the theory (3), assumed to be governing cosmological dynamics. Indeed, as [69] point out, generic Lorentz-invariant UV completions that come in at scales parametrically smaller than Λ_3 will bring

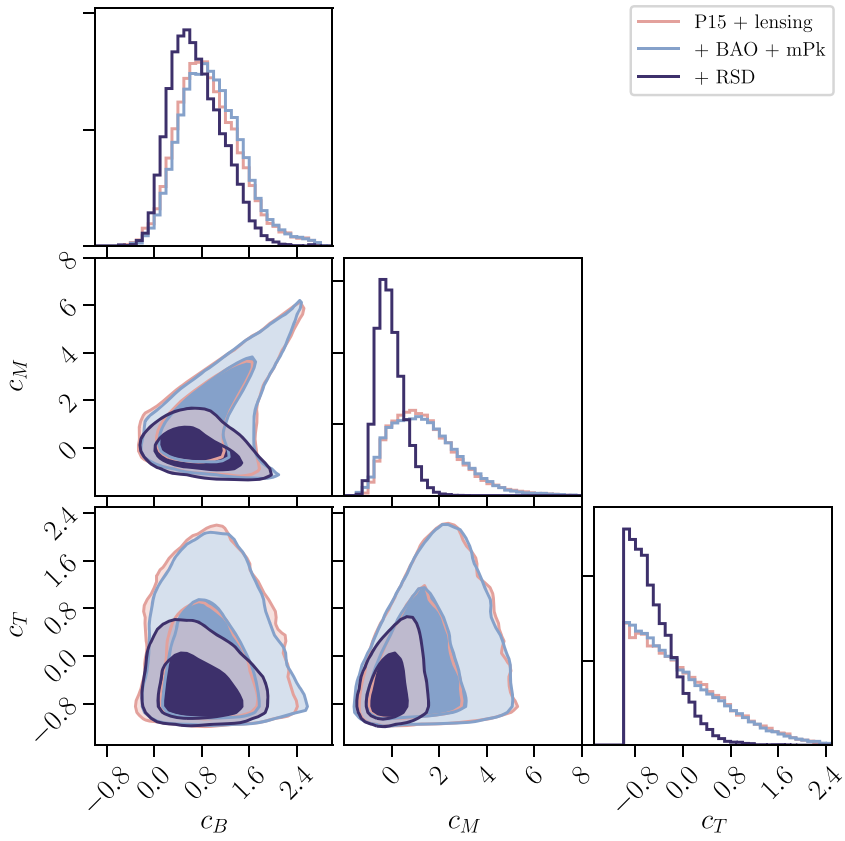

FIG. 5. Cosmological parameter constraints for the $\alpha_i = c_i\Omega_{\rm DE}$ parametrization, allowing α_T to vary as well. The inner (outer) contours correspond to 68% (95%) confidence levels, respectively. Note that constraints in the c_M, c_B plane are very similar to those obtained with a fixed $c_T = 0$ in Fig. 1—see Fig. 6 for a direct comparison. Note that, with the addition of RSD measurements, there is a preference for subluminal $c_{\rm GW}$ at the 1.6σ level—cf. Table II and recall that α_T here satisfies $c^2_{\rm GW} = c^2(1+\alpha_T) = c^2(1+c_T\Omega_{\rm DE})$.

a potentially subluminal cosmological speed of GWs back to luminal for the frequencies observed for GW170817. This argument subtly depends on the energy scale(s) associated to such a UV completion, so we refer to [20,69] for a detailed discussion of the naturalness of such a scenario—also see [68]. In any case, the large separation in the energy scales of cosmology and those probed by LIGO motivates exploring the cosmology-intrinsic bounds when also varying c_T. In this way any conclusion reached does not rely on the properties of a (partial) UV completion of the cosmological theory under consideration.

In this section we therefore discuss the constraints from the datasets introduced in Sec. IV on the full Horndeski theory (1), which also allows for a varying α_T. We compute constraints for the $\alpha_i = c_i\Omega_{\rm DE}$ parametrization and impose $c_T \geq -1$ to avoid unphysical, imaginary speeds for gravitational waves (this follows from the gradient (in)stability requirement $\alpha_T \geq -1$). These constraints are shown in Fig. 5. First of all notice that contours in the c_M, c_B plane are only mildly changed from the case with fixed $c_T = 0$, presented in Fig. 1(a). We explicitly compare these two cases in Fig. 6, which shows that the primary difference is due to the fact that a nonzero c_T somewhat shifts the gradient stability condition (14), allowing additional viable cosmologies with mildly negative c_M. The overall nature of the constraints on c_M and c_B, however, is relatively independent of the (non)evolution of c_T (at least for this parametrization). These constraints therefore appear rather robust (under prior changes for c_T). The addition of RSD data interestingly significantly drives down allowed values of c_T, with a preference for negative values and hence subluminal propagation of gravitational waves. In this context, note that known bounds on subluminal $c_{\rm GW}$ from the observation of high energy cosmic rays [70] probe energy scales even larger than LIGO, so should also be ignored in a cosmological context, if the GW170817 constraint is set aside for a cosmological analysis using the above reasoning.[22] In fact, the preference for a subluminal $c_{\rm GW}$ from the data aligns nicely with the theoretical observation, that the existence of a standard UV completion rules out superluminal speeds for the propagation of tensor or scalar perturbations (see e.g., [71,72]).

[22]From this perspective it would also be interesting to revisit indirect constraints from the energy loss of binary pulsars [31].

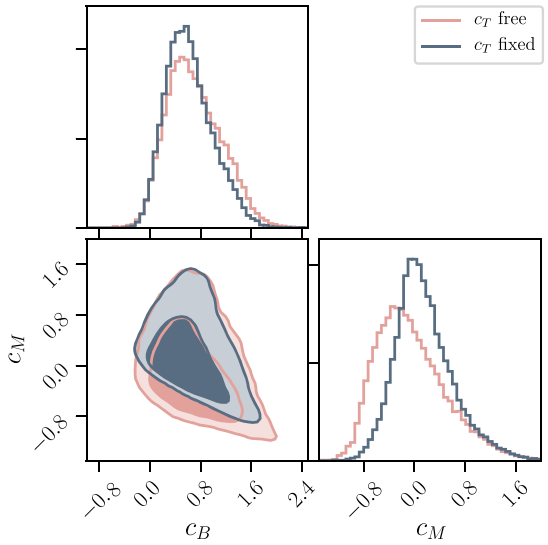

FIG. 6. Comparison of constraints for c_M and c_B using the $\alpha_i = c_i\Omega_{\rm DE}$ parametrization, contrasting the case of a fixed luminal speed of gravitational waves ($c_T = 0$) vs. the analogous constraints when that speed is allowed to vary. The inner (outer) contours correspond to 68% (95%) confidence levels, respectively. Here we use the full P15 + lensing + BAO + mPk + RSD dataset. Note that, in the $c_M - c_B$ plane, the primary effect of allowing c_T to vary is that the lower boundaries are extended, which is directly related to the fact that a varying c_T affects the onset of gradient instabilities [cf. Eq. (14)] and allows additional cosmologies with mildly negative c_M to avoid developing such instabilities.

Finally, let us briefly compare the constraints in Fig. 5 with those of Ref. [42], which performed a similar analysis, with two important differences. First, [42] use a much larger catalogue of RSD measurements than we do here (9 such measurements of $f\sigma_8$ compared to the two used here). We choose this conservative approach in order to safeguard against potential cross-correlations. Second, [42] treat the initial Planck mass as a free parameter, whereas we fix the initial Planck mass to be $M_{\rm Pl}$, as we are interested in late-universe modified gravity/dark energy effects here and do not wish to simultaneously constrain modifications at early times. Keeping these two points in mind and comparing the constraints from our Fig. 5 with Fig. 3 of [42], we obtain similar features for c_B, but the constraints on c_M differ as [42] prefer lower values of c_M. However, this is expected for the following two reasons: First, as discussed above, RSD data tend to prefer lower values of c_M, so it makes sense that adding more RSD measurements and assuming that they are independent strengthens this preference for low c_M. Note that [42] in fact prefer negative values for c_M (and hence a continuously decreasing effective Planck mass in cosmology) at $> 2\sigma$, whereas there is no such preference for negative c_M for our datasets. In this context it would be interesting to further investigate potential cross-correlations between the different RSD measurements, as well as possible correlations between RSDs and BAOs. Second, their analysis does not fix the initial value of the effective Planck mass and preferentially samples larger initial values for $M_{\rm Pl}$, which can be partially compensated for by reducing α_M. Given the tightly constrained range of allowed initial values for $M_{\rm Pl}$ found by [42], we however expect this second effect to be subdominant. Finally, [42] also observe a preference of the data for subluminal $c_{\rm GW}$, i.e. negative c_T.

VII. CONCLUSIONS

In this paper we have investigated cosmological parameter constraints for general Horndeski scalar-tensor theories, using CMB, redshift space distortion, matter power spectrum and BAO measurements from the Planck, SDSS/BOSS and 6dF surveys. We have focused on computing new constraints for models with luminally propagating gravitational waves (i.e. $c_{\rm GW} = c$ as e.g., motivated by the recent measurements from GW170817 and the assumption of a frequency-independent $c_{\rm GW}$), implementing and discussing several previously unaccounted for aspects in the constraint derivation for such theories. These include a careful handling of stability conditions, restricting the datasets included to safeguard against a potential contamination of results by unaccounted for cross-correlations and taking into account modified gravity effects on the computation of $f\sigma_8$ (and hence on extracting RSD constraints). Together they have strong qualitative effects on the constraints obtained. Extracting cosmological parameter constraints for any of the above models always requires choosing a parametrization for the residual functional freedom in such models—at the level of linear cosmology these are the α_i defined in (4). To avoid erroneously identifying artefacts of these parametrizations as features of the models to be tested, we compared results for three different parametrizations of the free functions in Horndeski scalar-tensor theories and identified parametrization-independent features of the constraints. The main constraints are shown in Figs. 1 and 2 for three different parametrizations of the α_i: $\alpha_i = c_i\Omega_{\rm DE}$, $\alpha_i = c_i a$ and $\alpha_i = c_i a^{n_i}$, where all c_i and n_i are constants. Finally, we also investigated models, where $c_{\rm GW}$ is treated as a free function for cosmology (motivated by the fact that the stringent constraints on $c_{\rm GW}$, such as from GW170817, measure this speed at energy scales/frequencies far removed from those relevant for cosmology) and discussed how this affects constraints—see Figs. 5 and 6. Key findings are the following:

(i) The running of the Planck mass, α_M, is tightly constrained in models where $c_{\rm GW} = c$. Depending on the parametrization, it can at most be mildly negative, due to strong gradient instabilities that plague models with an effective cosmological Planck mass significantly smaller than $M_{\rm Pl}$. Complementarily, RSD constraints strongly disfavor models with large positive α_M. In models where $\alpha_M \propto \alpha_B$, RSD constraints also break degeneracy directions in the

associated $c_M - c_B$ plane, exhibited by CMB constraints alone. α_B is preferentially driven to take positive values in all parametrizations.

(ii) CMB constraints are driven by the late ISW effect, with large regions of modified gravity parameter space ruled out by too much power in the TT CMB power spectra on large scales—see Fig. 3 and notice previous discussions of this effect in [40,49]. RSD measurements are the second main driver of constraints and act via placing tight bounds on $f\sigma_8$, where fully modeling dark energy/modified gravity effects is crucial in order to extract the maximal constraining power.

(iii) GR is consistent with the parameter constraints derived here at $\sim 2\sigma$ (see Table II for parametrization-specific values). At the level of the "modified gravity functions" α_i, any preference for departures from GR is typically driven by the braiding function α_B.

(iv) For models with $c_{\rm GW} \neq c$ in a cosmological setting (still allowed by GW170817 for a frequency-dependent $c_{\rm GW}$—see [69] and the discussion in Sec. VI), we show constraints in Fig. 5. Jointly using CMB and RSD data leads to a 1.6σ preference for subluminally propagating gravitational waves in cosmology—cf. related constraints in [42].

(v) Constraints on α_M and α_B are mildly affected by freeing up $c_{\rm GW}$ (at least for the parametrization tested—see Fig. 6) in an interesting way. Due to a modified gradient stability condition, additional viable cosmologies with negative α_M are present in this case.

Several future extensions of the work presented here suggest themselves, especially related to the addition of further observational and/or theoretical constraints. On the observational front, local constraints e.g., from lunar laser ranging [73,74], may place additional strong constraints for models that have a sufficiently large cutoff (such that the energy scales tested by such local tests are within the regime of validity of the theory). "Standard sirens" associated to future gravitational wave observations will also yield further constraints (see e.g., [75,76] and references therein). At larger scales e.g., additional RSD measurements (cf. [42]), weak lensing data and galaxy-ISW cross-correlations (cf. [30,77,78]) promise to add additional constraining power for testing deviations from GR. On the theoretical front, e.g., a better understanding of constraints from radiative stability [67] and positivity bounds [71,72] for gravitational scalar-tensor theories will help in further narrowing down the range of allowed models. By reducing the inherent functional freedom in modified gravity and dark energy theories this will also improve observational bounds on such theories in the process [67]. The work presented here will hopefully be a useful stepping stone for such future extensions, establishing a number of robust constraints on dark energy and modified gravity models with current data.

ACKNOWLEDGMENTS

We especially thank E. Bellini for numerous discussions and shared insights. We also acknowledge several useful discussions with T. Brinckmann, P. Ferreira, E. Komatsu, C. Kreisch and A. Refregier. J. N. acknowledges support from Dr. Max Rössler, the Walter Haefner Foundation and the ETH Zurich Foundation. A. N. acknowledges support from SNF Grant No. 200021_169130. In deriving the results of this paper, we have used: CLASS [61], CORNER [79], HI_CLASS [40], MONTEPYTON [62,63], XACT [80] and XIST [81].

APPENDIX A: THEORETICAL MODELING OF OBSERVATIONS: IMPLEMENTATION DETAILS

RSD: Redshift space distortions measure the anisotropic clustering of galaxies in redshift space and are sensitive to the parameter combination $f(z_{\rm eff})\sigma_8(z_{\rm eff})$, where $f(z_{\rm eff})$ is the logarithmic linear growth rate, and $\sigma_8(z_{\rm eff})$ is the rms of matter fluctuations in spheres of radius 8 h^{-1} Mpc at the effective redshift of the galaxy sample $z_{\rm eff}$. In GR, the expression for the logarithmic linear growth rate is given by

$$f(z_{\rm eff}) = \frac{{\rm d}\log D}{{\rm d}\log a}, \tag{A1}$$

where D is the growth factor. Within GR, the growth factor D can be estimated using the Heath integral [82] for ΛDCM cosmologies or by solving a GR-specific differential equation for late-time matter perturbations (also valid for a number of minimally coupled dark energy cosmologies—see e.g., [83]). These two approaches are not valid for general modified gravity theories and we therefore estimate $f(z_{\rm eff})$ through

$$f(z_{\rm eff}) = \left.\frac{{\rm d}P^{1/2}_{mm,{\rm lin}}(k,a)}{{\rm d}\log a}\right|_{k=k_{\rm fid}}. \tag{A2}$$

We evaluate (A2) at a fiducial wave vector value $k_{\rm fid}$ using a three-point numerical derivative. As the linear growth rate is defined to be manifestly scale-independent, we choose a fiducial wave vector value such that we can approximate $f(z_{\rm eff})$ as scale-independent. Specifically, we consider the dependence of f on k at a fixed redshift. As shown in Fig. 7(b), we find the growth rate to be relatively scale-independent for general Horndeski models, except at large scales. We therefore choose a fiducial wave vector well in the scale-independent regime, i.e. $k_{\rm fid} = 0.05$ Mpc^{-1}.[23]

Note that the issue of scale-dependence is also related to the observational modeling required to extract

[23]We note that, be default, the growth factor D is computed using the Heath integral within HI_CLASS and it is thus important to implement the approach outlined above in order to capture all modified gravity effects. We thank Emilio Bellini for pointing this out to us.

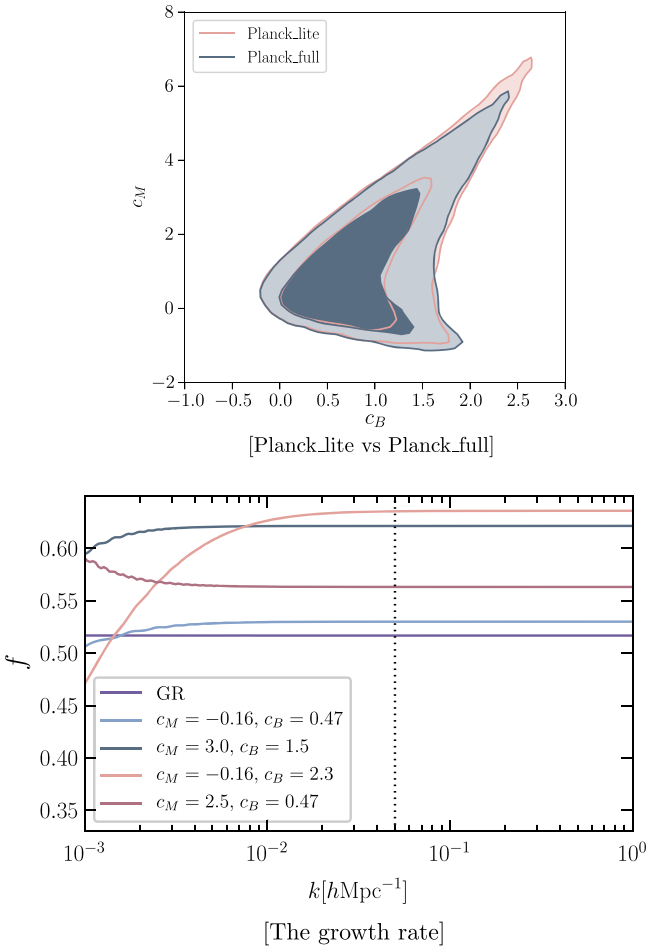

FIG. 7. (a) Comparison of constraints from P15 + lensing, where the high-ℓ likelihood used is either the premarginalized high-ℓ PLIK LITE temperature likelihood or the full high-ℓ temperature likelihood. We have marginalized over all other cosmological and nuisance parameters here. The two results agree very well. (b) Illustration of the growth rate f as a function of wave vector k for a fiducial cosmological model with various choices of c_i for the parametrization (7). The vertical line shows our fiducial wave vector $k_{\rm fid} = 0.05$ Mpc^{-1}. We emphasize that the growth rate becomes scale-independent for $k \geq k_{\rm fid}$ for all cosmologies probed here.

measurements of $f\sigma_8$ from galaxy surveys, which are typically constructed based on GR and validated using GR mock catalogues. Comparison with dedicated Dvali-Gabadadze-Porrati mock catalogues (displaying scale-independent linear growth) showed that using the standard $f\sigma_8$ measurements remains appropriate at least for these models [84]. On the other hand, at least for some models with scale-dependent linear growth a more dedicated observational modeling is required to extract the correct $f\sigma_8$ measurements for such theories [85].[24]

[24]We thank Alex Barreira for related discussions.

mPk: The matter power spectrum at small scales is affected by nonlinear clustering and potential scale-dependent galaxy bias. Reference [9] model these effects using the fitting formula derived in Ref. [86]. This expression parametrizes the relation between linear matter power spectrum and nonlinear galaxy power spectrum, calibrated from N-body simulations. Furthermore, Ref. [9] also take into account the BAO smoothing due to nonlinear evolution. In this work, we choose an alternative approach following Ref. [87]: as shown in Ref. [87], the smoothing of BAO peaks does not significantly affect the derived constraints on cosmological parameters and we therefore do not include this effect into our analysis. Furthermore, we choose to model the galaxy power spectrum $P_{gg}(k)$ as in Ref. [87] i.e.

$$P_{gg}(k) = b^2 P_{mm}^{\rm nonlin}(k) + n. \tag{A3}$$

The quantity $P_{mm}^{\rm nonlin}(k)$ is the nonlinear matter power spectrum, b denotes a linear galaxy bias parameter and n parametrizes systematic uncertainties due to shot noise and nonlinear evolution. It has been shown in Ref. [87] that the model given in Eq. (A3) gives parameter constraints consistent with Ref. [9], while being motivated from perturbation theory. In our work, we model $P_{mm}^{\rm nonlin}(k)$ using the revised HALOFIT fitting function [88,89]. We note that HALOFIT does not include modified gravity effects on the nonlinear matter power spectrum. However, corrections due to nonlinear clustering are small for the wave vector ranges considered in this work and can be captured by the nuisance parameter n. As the addition of the matter power spectrum does not significantly modify the derived constraints on modified gravity parameters (they are driven by Planck and RSD data), we thus believe this choice to not affect our conclusions. When estimating constraints on cosmological parameters, we finally marginalize over b and n.

APPENDIX B: ADDITIONAL CONSTRAINTS AND CONSISTENCY CHECKS

Planck temperature high-ℓ *likelihoods*: In Fig. 7(a) we show a comparison of pure Planck 2015 constraints on the c_i parameters of the $\alpha_i = c_i \Omega_{\rm DE}$ parametrization obtained using the full Planck high-ℓ temperature likelihood (with all of its additional nuisance parameters—16 in total) vs. the premarginalized PLIK LITE likelihood (which has one nuisance parameter). These two sets of constraints agree very well, justifying the use of the PLIK LITE likelihood in the derivation of the constraints shown throughout the majority of this paper. Note that the PLIK LITE likelihood has been premarginalized assuming a ΛCDM cosmology, so the fact that we find good agreement is at least partially due to our choice of a ΛCDM background cosmology throughout this paper and, in that sense, unsurprising. If

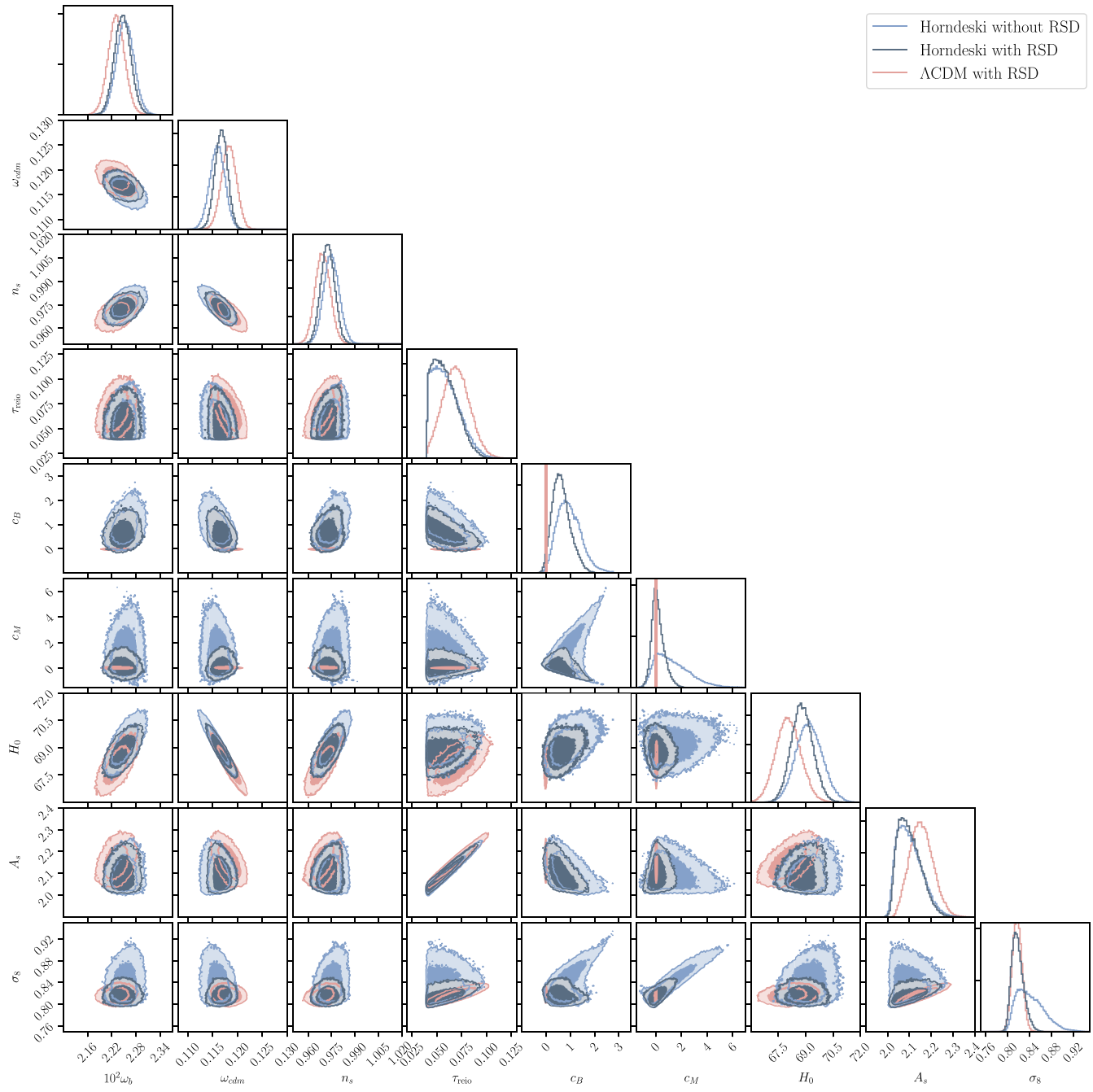

FIG. 8. Cosmological parameter constraints for all ΛCDM cosmological parameters in addition to the modified gravity/dark energy c_i parameters, using parametrization (7) for the "Horndeski" contours. For comparison we also show the constraints obtained for a standard ΛCDM model without any additional degrees of freedom. Nuisance parameters are marginalized over and not shown in both cases. As datasets we use P15 + lensing + BAO + mPk data vs. the same dataset with additional RSD data, all as described in Sec. IV. Pure ΛCDM contours are only very mildly affected by the addition of the two RSD measurements we use, so we only plot constraints for the combined datasets in that case.

different background cosmologies are explored, more caution ought to be exercised in using the PLIK LITE likelihood.

Constraints on other cosmological parameters: Throughout this paper we have focused on constraints for the modified gravity and dark energy parameters as captured by the α_i and their respective parametrizations. In Fig. 8 we now for completeness also show constraints for the standard cosmological ΛCDM parameters for one of the parametrizations used, namely $\alpha_i = c_i\Omega_{\rm DE}$. Here we show constraints obtained using P15 + lensing + BAO + mPk data and constraints obtained once RSD data are added.

TABLE III. Common parameters varied in the MCMC analysis for the different parametrizations used in this paper with their respective priors and posteriors. The uncertainties shown denote the 95% confidence level. $A_{\rm Planck}$, b and n are nuisance parameters. Param I* refers to parametrization I with a varying c_T. The $c_M/c_{\delta M}$ row shows posteriors for $c_{\delta M}$ for parametrization III and for c_M for all other parametrizations.

Parameter	Prior	Param. I	Param. II	Param. III	Param. I*
$100\theta_{\rm s}$	Flat unbound	2.25 ± 0.04	2.24 ± 0.04	2.24 ± 0.04	2.25 ± 0.04
$w_{\rm cdm}$	Flat unbound	$0.117^{+0.002}_{-0.003}$	0.117 ± 0.003	0.117 ± 0.003	0.117 ± 0.003
$w_{\rm b}$	Flat unbound	0.0104 ± 0.0008	0.0104 ± 0.0008	0.0104 ± 0.0008	0.0104 ± 0.0008
$n_{\rm s}$	Flat unbound	0.973 ± 0.009	0.972 ± 0.009	0.972 ± 0.009	0.973 ± 0.009
$\log 10^{10} A_{\rm s}$	Flat unbound	$3.05^{+0.053}_{-0.037}$	$3.05^{+0.06}_{-0.05}$	3.06 ± 0.05	$3.04^{+0.05}_{-0.04}$
$\tau_{\rm reion}$	Flat $\in [0.04, -]$	$0.0588^{+0.0276}_{-0.0177}$	$0.0662^{+0.0302}_{-0.0239}$	$0.0677^{+0.0267}_{-0.0237}$	$0.0588^{+0.0280}_{-0.0177}$
$c_M/c_{\delta M}$	Flat unbound	$0.20^{+1.15}_{-0.82}$	$0.27^{+0.54}_{-0.26}$	$0.30^{+0.77}_{-0.45}$	$-0.01^{+1.30}_{-0.87}$
c_B	Flat unbound	$0.63^{+0.83}_{-0.62}$	$0.48^{+0.83}_{-0.46}$	$1.1^{+0.89}_{-1.10}$	$0.71^{+0.88}_{-0.71}$
$A_{\rm Planck}$	Flat $\in [0.9, 1.1]$	1.00 ± 0.5	1.00 ± 0.5	1.00 ± 0.5	1.00 ± 0.5
b	Flat $\in [1., 3.]$	2.19 ± 0.06	$2.16^{+0.10}_{-0.12}$	$2.19^{+0.09}_{-0.11}$	$2.22^{+0.11}_{-0.13}$
n	Flat $\in [0., 21390.]$	$1494.^{+3000.}_{-1430.}$	$1427.^{+2764.}_{-1360.}$	$1434.^{+2862.}_{-1374.}$	$1477.^{+2913.}_{-1415.}$

Figure 1(a) then is essentially a zoom-in on the c_M, c_B of Fig. 8, so those constraints are of course identical. For comparison we also show constraints on the ΛCDM parameters obtained for a vanilla ΛCDM model without any additional degrees of freedom and for the same datasets. In terms of the ΛCDM parameters in modified gravity/dark energy models, the main effect of adding RSD data is on σ_8 and H_0. Both are pushed towards lower values by adding RSD data. In the case of H_0 this shift is only mild and still leads to a best-fit H_0 larger than in the pure ΛCDM case. For σ_8 the shift is more notable and one can also notice a "degeneracy direction" in the $c_M - \sigma_8$ plane for CMB + BAO + mPk constraints, that is broken by adding RSD measurements. This is because σ_8 effectively controls the number density of collapsed objects at a given scale. If c_M increases, this means the effective Planck mass at late

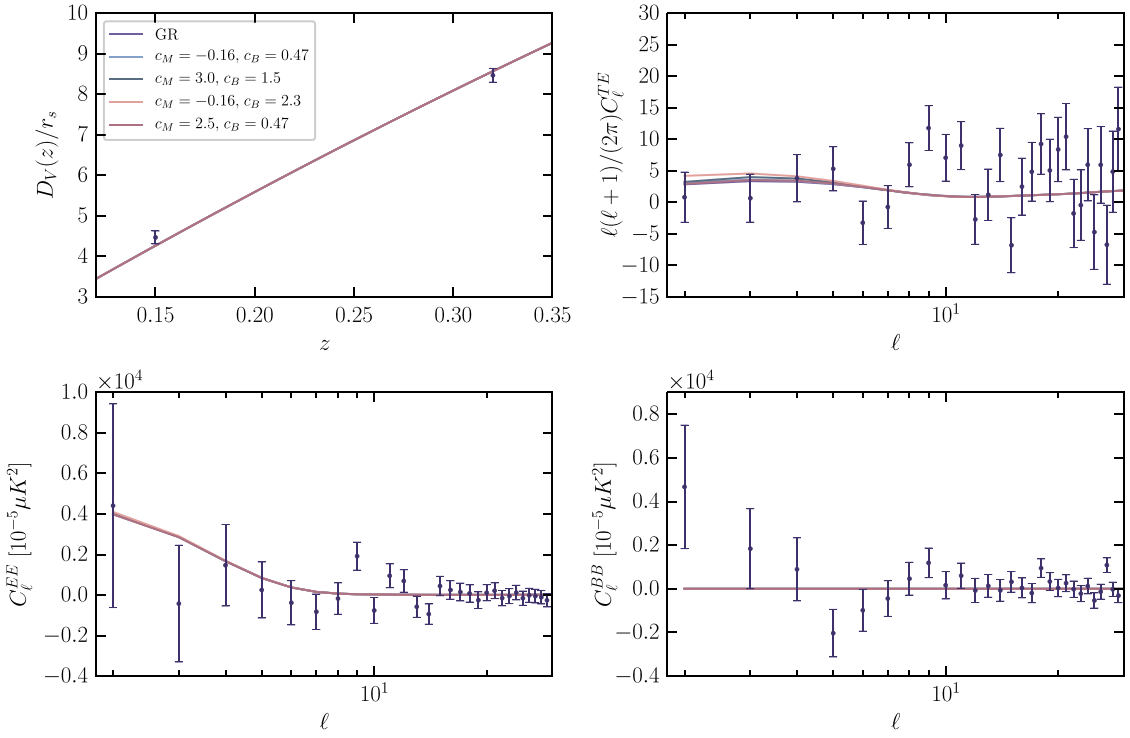

FIG. 9. Illustration of the BAO (top left) and CMB data used in this work (note that the C_l^{TT} are shown in Fig. 3). The cosmologies plotted are the same as in Figs. 3 and 4 and the results here should be seen as consistency checks—as discussed in Appendix B, one does not expect there to be any strong signal of modified gravity effects for the observables plotted here.

times increases, so gravity is stronger and objects collapse more efficiently. So it makes sense that these two parameters are correlated. However, while increasing c_M increases σ_8 at low redshifts (σ_8 in Fig. 8 is measured at redshift zero), at redshifts relevant for CMB constraints different values of c_M have almost no effect on σ_8. This explains why both σ_8 measured at redshift zero and c_M are only relatively weakly constrained by CMB(+BAO + mPk) measurements. Adding RSD data then adds additional and direct sensitivity to the late-universe effects of c_M (and σ_8), reducing c_M and bringing the posterior for σ_8 into excellent agreement with the one derived from standard ΛCDM. Finally, there are also small differences for $\omega_{\rm cdm}$ and n_s, which can both be understood in terms of their correlation with H_0, i.e. this correlation drives the mild differences in those parameters. Note that, motivated by observations of the Gunn-Peterson trough (see e.g., [90]), we impose a prior $\tau_{\rm reion} \geq 0.04$, corresponding to $z_{\rm reion} \gtrsim 6$. In Table III we furthermore collect parameter constraints for the common parameters varied in all parametrizations for the full P15 + lensing + BAO + mPk + RSD dataset.

Additional CMB and BAO constraints: In Fig. 9 we show the remaining constraints from BAOs and the other CMB power spectra for the same cosmologies as shown in Figs. 3 and 4 as consistency tests. The BAO measurement of $D_V(z)/r_s$, being a background measurement, unsurprisingly does not discriminate between cosmologies with the same ΛCDM background cosmology (but different perturbations controlled by the c_i parameters). The BB power spectrum is identically zero, since we have set the (primordial) tensor-to-scalar ratio $r = 0$ and the additional scalar modes in Horndeski ST theories do not source tensor/B modes. E modes are also hardly affected at all, so this is a good consistency check that almost all of the CMB constraining power does indeed come from the scalar modes (as thoroughly probed by the T modes), which are modified in the theories we investigate here.

[1] G. W. Horndeski, Int. J. Theor. Phys. **10**, 363 (1974).
[2] C. Deffayet, X. Gao, D. A. Steer, and G. Zahariade, Phys. Rev. D **84**, 064039 (2011).
[3] (Planck Collaboration)), Astron. Astrophys. **594**, A13 (2016).
[4] (Planck Collaboration), Astron. Astrophys. **594**, A15 (2016).
[5] L. Anderson *et al.*, Mon. Not. R. Astron. Soc. **441**, 24 (2014).
[6] A. J. Ross, L. Samushia, C. Howlett, W. J. Percival, A. Burden, and M. Manera, Mon. Not. R. Astron. Soc. **449**, 835 (2015).
[7] F. Beutler, C. Blake, M. Colless, D. H. Jones, L. Staveley-Smith, G. B. Poole, L. Campbell, Q. Parker, W. Saunders, and F. Watson, Mon. Not. R. Astron. Soc. **423**, 3430 (2012).
[8] L. Samushia *et al.*, Mon. Not. R. Astron. Soc. **439**, 3504 (2014).
[9] M. Tegmark *et al.*, Phys. Rev. D **74**, 123507 (2006).
[10] J. Gleyzes, D. Langlois, F. Piazza, and F. Vernizzi, Phys. Rev. Lett. **114**, 211101 (2015).
[11] D. Langlois and K. Noui, J. Cosmol. Astropart. Phys. 02 (2016) 034.
[12] J. Ben Achour, M. Crisostomi, K. Koyama, D. Langlois, K. Noui, and G. Tasinato, J. High Energy Phys. 12 (2016) 100.
[13] T. Kobayashi, M. Yamaguchi, and J. Yokoyama, Prog. Theor. Phys. **126**, 511 (2011).
[14] B. P. Abbott *et al.* (LIGO Scientific and Virgo Collaborations), Phys. Rev. Lett. **119**, 161101 (2017).
[15] A. Goldstein *et al.*, Astrophys. J. Lett. **848**, L14 (2017).
[16] V. Savchenko *et al.*, Astrophys. J. Lett. **848**, L15 (2017).
[17] B. P. Abbott *et al.*, Astrophys. J. Lett. **848**, L13 (2017).
[18] B. P. Abbott *et al.*, Astrophys. J. Lett. **848**, L12 (2017).
[19] T. Baker, E. Bellini, P. G. Ferreira, M. Lagos, J. Noller, and I. Sawicki, Phys. Rev. Lett. **119**, 251301 (2017).
[20] P. Creminelli and F. Vernizzi, Phys. Rev. Lett. **119**, 251302 (2017).
[21] J. Sakstein and B. Jain, Phys. Rev. Lett. **119**, 251303 (2017).
[22] J. M. Ezquiaga and M. Zumalacárregui, Phys. Rev. Lett. **119**, 251304 (2017).
[23] C. Deffayet, O. Pujolas, I. Sawicki, and A. Vikman, J. Cosmol. Astropart. Phys. 10 (**2010**) 026.
[24] L. Amendola, M. Kunz, M. Motta, I. D. Saltas, and I. Sawicki, Phys. Rev. D **87**, 023501 (2013).
[25] L. Amendola, G. Ballesteros, and V. Pettorino, Phys. Rev. D **90**, 043009 (2014).
[26] E. V. Linder, Phys. Rev. D **90**, 083536 (2014).
[27] M. Raveri, C. Baccigalupi, A. Silvestri, and S.-Y. Zhou, Phys. Rev. D **91**, 061501 (2015).
[28] I. D. Saltas, I. Sawicki, L. Amendola, and M. Kunz, Phys. Rev. Lett. **113**, 191101 (2014).
[29] L. Lombriser and A. Taylor, J. Cosmol. Astropart. Phys. 03 (2016) 031.
[30] L. Lombriser and N. A. Lima, Phys. Lett. B **765**, 382 (2017).
[31] J. Beltran Jimenez, F. Piazza, and H. Velten, Phys. Rev. Lett. **116**, 061101 (2016).
[32] D. Bettoni, J. M. Ezquiaga, K. Hinterbichler, and M. Zumalacarregui, Phys. Rev. D **95**, 084029 (2017).
[33] I. Sawicki, I. D. Saltas, M. Motta, L. Amendola, and M. Kunz, Phys. Rev. D **95**, 083520 (2017).
[34] E. Bellini and I. Sawicki, J. Cosmol. Astropart. Phys. 07 (2014) 050.
[35] J. Gleyzes, D. Langlois, F. Piazza, and F. Vernizzi, J. Cosmol. Astropart. Phys. 08 (**2013**) 025.

[36] M. Lagos, T. Baker, P. G. Ferreira, and J. Noller, J. Cosmol. Astropart. Phys. 08 (2016) 007,
[37] M. Lagos, E. Bellini, J. Noller, P. G. Ferreira, and T. Baker, J. Cosmol. Astropart. Phys. 03 (2018) 021.
[38] G. Gubitosi, F. Piazza, and F. Vernizzi, J. Cosmol. Astropart. Phys. 02 (2013) 032.
[39] J. K. Bloomfield, E. E. Flanagan, M. Park, and S. Watson, J. Cosmol. Astropart. Phys. 08 (**2013**) 010.
[40] M. Zumalacárregui, E. Bellini, I. Sawicki, J. Lesgourgues, and P. G. Ferreira, J. Cosmol. Astropart. Phys. 08 (2017) 019.
[41] B. Hu, M. Raveri, N. Frusciante, and A. Silvestri, Phys. Rev. D **89**, 103530 (2014).
[42] E. Bellini, A. J. Cuesta, R. Jimenez, and L. Verde, J. Cosmol. Astropart. Phys. 02 (**2016**) 053; 06 (2016) E01.
[43] D. Alonso, E. Bellini, P. G. Ferreira, and M. Zumalacarregui, Phys. Rev. D **95**, 063502 (2017).
[44] E. V. Linder, G. Sengör, and S. Watson, J. Cosmol. Astropart. Phys. 05 (2016) 053.
[45] E. V. Linder, Phys. Rev. D **95**, 023518 (2017).
[46] J. Gleyzes, Phys. Rev. D **96**, 063516 (2017).
[47] M. Denissenya and E. V. Linder, J. Cosmol. Astropart. Phys. 11 (2018) 010.
[48] L. Lombriser, C. Dalang, J. Kennedy, and A. Taylor, J. Cosmol. Astropart. Phys. 01 (2019) 041.
[49] C. D. Kreisch and E. Komatsu, J. Cosmol. Astropart. Phys. 12 (2018) 030.
[50] S. Arai and A. Nishizawa, Phys. Rev. D **97**, 104038 (2018).
[51] N. Frusciante, S. Peirone, S. Casas, and N. A. Lima, Phys. Rev. D **99**, 063538 (2019).
[52] R. Reischke, A. S. Mancini, B. M. Schäfer, and P. M. Merkel, Mon. Not. R. Astron. Soc. **482**, 3274 (2019).
[53] A. S. Mancini, R. Reischke, V. Pettorino, B. M. Schäefer, and M. Zumalacárregui, Mon. Not. R. Astron. Soc. **480**, 3725 (2018).
[54] O. Pujolas, I. Sawicki, and A. Vikman, J. High Energy Phys. 11 (2011) 156.
[55] A. Barreira, B. Li, C. Baugh, and S. Pascoli, J. Cosmol. Astropart. Phys. 08 (2014) 059.
[56] A. E. Gümrükçüoğlu, S. Mukohyama, and T. P. Sotiriou, Phys. Rev. D **94**, 064001 (2016).
[57] A. De Felice, N. Frusciante, and G. Papadomanolakis, J. Cosmol. Astropart. Phys. 03 (**2017**) 027.
[58] N. Frusciante, G. Papadomanolakis, S. Peirone, and A. Silvestri, J. Cosmol. Astropart. Phys. 02 (2019) 029.
[59] (Planck Collaboration), Astron. Astrophys. **594**, A1 (2016).
[60] N. Aghanim *et al.* (Planck Collaboration), Astron. Astrophys. **594**, A11 (2016).
[61] D. Blas, J. Lesgourgues, and T. Tram, J. Cosmol. Astropart. Phys. 07 (2011) 034.
[62] B. Audren, J. Lesgourgues, K. Benabed, and S. Prunet, J. Cosmol. Astropart. Phys. 02 (**2013**) 001.
[63] T. Brinckmann and J. Lesgourgues, Phys. Rev. D **97**, 063506 (2018).
[64] N. Metropolis, A. W. Rosenbluth, M. N. Rosenbluth, A. H. Teller, and E. Teller, J. Chem. Phys. **21**, 1087 (1953).
[65] W. K. Hastings, Biometrika **57**, 97 (1970).
[66] A. Gelman and D. B. Rubin, Stat. Sci. **7**, 457 (1992).
[67] J. Noller and A. Nicola, arXiv:1811.03082.
[68] P. Creminelli, M. Lewandowski, G. Tambalo, and F. Vernizzi, J. Cosmol. Astropart. Phys. 12 (2018) 025.
[69] C. de Rham and S. Melville, Phys. Rev. Lett. **121**, 221101 (2018).
[70] G. D. Moore and A. E. Nelson, J. High Energy Phys. 09 (2001) 023.
[71] A. Adams, N. Arkani-Hamed, S. Dubovsky, A. Nicolis, and R. Rattazzi, J. High Energy Phys. 10 (2006) 014.
[72] C. de Rham, S. Melville, A. J. Tolley, and S.-Y. Zhou, Phys. Rev. D **96**, 081702 (2017).
[73] J. G. Williams, S. G. Turyshev, and D. H. Boggs, Phys. Rev. Lett. **93**, 261101 (2004).
[74] E. Babichev, C. Deffayet, and G. Esposito-Farese, Phys. Rev. Lett. **107**, 251102 (2011).
[75] J. M. Ezquiaga and M. Zumalacárregui, Front. Astron. Space Sci. **5**, 44 (2018).
[76] M. Lagos, M. Fishbach, P. Landry, and D. E. Holz, Phys. Rev. D **99**, 083504 (2019).
[77] J. Renk, M. Zumalacarregui, and F. Montanari, J. Cosmol. Astropart. Phys. 07 (2016) 040.
[78] J. Renk, M. Zumalacárregui, F. Montanari, and A. Barreira, J. Cosmol. Astropart. Phys. 10 (2017) 020.
[79] D. Foreman-Mackey, J. Open Source Softw. **1**, 24 (2016).
[80] J. M. Martín-García, http://www.xact.es/.
[81] J. Noller, https://github.com/xAct-contrib/xIST.
[82] D. J. Heath, Mon. Not. R. Astron. Soc. **179**, 351 (1977).
[83] S. Dodelson, *Modern Cosmology/Scott Dodelson* (Academic Press, Amsterdam, Netherlands, 2003), XIII, p. 440.
[84] A. Barreira, A. G. Sánchez, and F. Schmidt, Phys. Rev. D **94**, 084022 (2016).
[85] A. Taruya, K. Koyama, T. Hiramatsu, and A. Oka, Phys. Rev. D **89**, 043509 (2014).
[86] S. Cole *et al.*, Mon. Not. R. Astron. Soc. **362**, 505 (2005).
[87] J. Dunkley, E. Komatsu, M. R. Nolta, D. N. Spergel, D. Larson, G. Hinshaw, L. Page, C. L. Bennett, B. Gold, N. Jarosik, J. L. Weiland, M. Halpern, R. S. Hill, A. Kogut, M. Limon, S. S. Meyer, G. S. Tucker, E. Wollack, and E. L. Wright, Astrophys. J. Suppl. Ser. **180**, 306 (2009).
[88] R. E. Smith, J. A. Peacock, A. Jenkins, S. D. M. White, C. S. Frenk, F. R. Pearce, P. A. Thomas, G. Efstathiou, and H. M. P. Couchman, Mon. Not. R. Astron. Soc. **341**, 1311 (2003).
[89] R. Takahashi, M. Sato, T. Nishimichi, A. Taruya, and M. Oguri, Astrophys. J. **761**, 152 (2012).
[90] R. H. Becker *et al.* (SDSS Collaboration), Astron. J. **122**, 2850 (2001).